Tectonics

RESEARCH ARTICLE
10.1029/2018TC005298

Thermotectonic Evolution of the North Pyrenean Agly Massif During Early Cretaceous Hyperextension Using Multi-mineral U-Pb Thermochronometry

M. L. Odlum[1] and **D. F. Stockli**[1]

[1]Department of Geological Sciences, Jackson School of Geosciences, University of Texas at Austin, Austin, TX, USA

Key Points:
- High-temperature thermochronometers record the preorogenic, Early Cretaceous rifting and hyperextension in the Eastern Pyrenees
- Apatite U-Pb thermochronometry distinguishes between decoupled and coupled extension constrains exhumation of the middle-lower crust
- The Agly Massif provides important and transportable insights into the temporal, thermal, and geometric evolution of rifted margins

Supporting Information:
- Supporting Information S1
- Figure S1
- Data Set S1
- Data Set S2
- Data Set S3
- Data Set S4
- Data Set S5
- Data Set S6
- Data Set S7

Correspondence to:
M. L. Odlum,
modlum@utexas.edu

Citation:
Odlum, M. L., & Stockli, D. F. (2019). Thermotectonic evolution of the North Pyrenean Agly Massif during Early Cretaceous hyperextension using multi-mineral U-Pb thermochronometry. *Tectonics*, *38*, 1509–1531. https://doi.org/10.1029/2018TC005298

Received 24 AUG 2018
Accepted 10 MAR 2019
Accepted article online 18 MAR 2019
Corrected 29 MAY 2019
Published online 2 MAY 2019

This article was corrected on 29 MAY 2019. See the end of the full text for details.

Abstract The North Pyrenean Zone represents a fossil hyperextended passive margin, with limited orogenic overprinting, where the thermal and structural patterns associated with crustal thinning and mantle exhumation can be studied on rocks exposed at the surface. The Agly Massif is a tilted ~10-km-thick crustal section of Paleozoic and upper Proterozoic magmatic and greenschist to granulitic metamorphic rocks in the easternmost North Pyrenean Zone. We applied multi-mineral geochronometry and thermochronometry on structural/crustal transects across the massif to understand the exhumation history of the upper and lower continental crust during extreme crustal thinning and mantle exhumation. Integration of zircon and apatite U-Pb ages provides unprecedented constraints to understand the decoupled versus coupled extensional evolution, exhumation timing of the middle-lower crust, and the age of juxtaposition of the upper crust granitic pluton with high-grade gneisses. The Saint Arnac pluton was emplaced and cooled in the upper crust during the Carboniferous and remained at temperatures between 450 and 180 °C until the Late Cretaceous. The middle to lower crust was metamorphosed during the Carboniferous and remained at temperatures >450 °C until the Aptian, when it was rapidly exhumed along a midcrustal shear zone. Deformation was initially decoupled along a midcrustal ductile shear zone until the whole massif was in the brittle field, with structural juxtaposition of the units, and exhumation was coupled and controlled by a major southward dipping detachment fault at the southern border of the massif. The basement massif and synrift sedimentary rocks record significantly different thermal histories during rifting.

1. Introduction

Studies over the past several decades have advanced the understanding of the geometric, structural, and thermal evolution of magma-poor rifted margins (e.g., Beltrando et al., 2015; Clerc & Lagabrielle, 2014; Clerc et al., 2018; Davis & Kusznir, 2004; Huismans & Beaumont, 2008; Huismans & Beaumont, 2011; Manatschal, 2004; Mohn et al., 2012; Péron-Pinvidic et al., 2007; Reston, 2009; Whitmarsh et al., 2001). Recently, improved technologies allowing for better resolution seismic reflection and refraction imaging, especially of the lower crust, have led to reconsideration of classical and numerical models of rifting mechanisms and highlighted the striking diversity in the geometry of the rifted margins observed worldwide (Clerc et al., 2018).

Recent models invoke different extensional mechanisms for the formation of magma-poor rifted margins such as ductile deformation of the lower crust (Brun & Beslier, 1996; Driscoll & Karner, 1998; Huismans & Beaumont, 2011, 2014; Jolivet et al., 2015), boudinage of the lower crust (Reston, 1988), three-layer continental crust with brittle upper and lower crust strongly decoupled by a ductile middle crust (Manatschal, 2004; Mohn et al., 2012; Lavier & Manatschal, 2006; Péron-Pinvidic et al. 2007; Péron-Pinvidic & Manatschal, 2009), and boudinage of the upper crust allowed by high thermal geothermal regime and blanketing effect of the decoupled prerift and synrift sedimentary strata (Clerc & Lagabrielle, 2014; Lagabrielle et al., 2016). These models lead to different predicted lithospheric architectures and thermal histories, and the diversity in observed rifted margins worldwide makes it impossible to use a single model for all rifted margins.

Direct constraints on processes associated with rifting and mantle exhumation, often necessary for discriminating between geodynamic models, are limited because most outcrops of rocks recording the evolution of modern rifted margins, especially at the distal margin, are in the marine realm. However, direct sampling of these rocks is possible in the fossil rift margin within the North Pyrenean Zone (NPZ), France, allowing for study of the architecture of rift margins, thermal histories of the continental crust, and the geodynamic processes during rifting/hyperextension and subcontinental mantle exhumation.

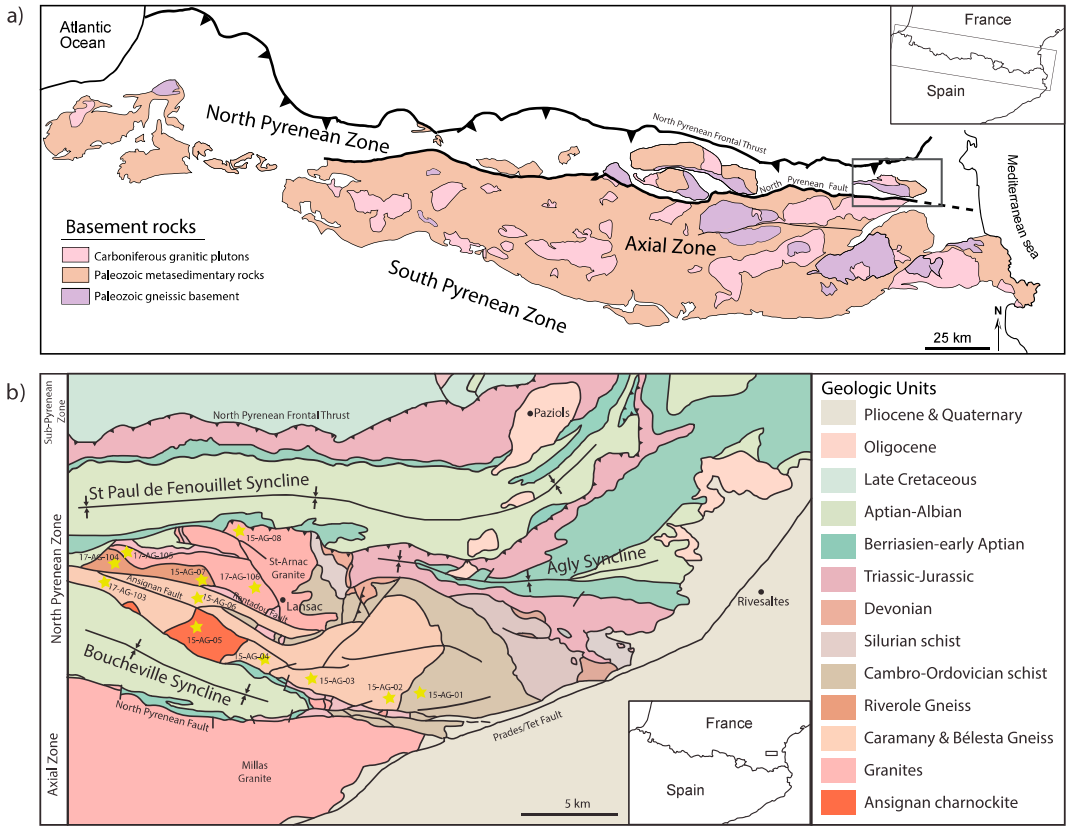

Figure 1. (a) Geological map of the magmatic and metamorphic rocks in the Pyrenees showing main Variscan aged plutons and gneiss domes (modified after Denèle et al., 2014). (b) Structural map of the Agly Massif modified after the BRGM map of Rivesaltes (Fonteilles et al., 1993) with samples indicated by yellow stars.

The NPZ (Choukroune, 1974) is a narrow fold-and-thrust belt composed of HT-LP metamorphosed sedimentary basins of the "Internal Metamorphic Zone" (Albarède & Michard-Vitrac, 1978; Golberg & Maluski, 1988; Golberg & Leyreloup, 1990; Lagabrielle et al., 2010), basement massifs, and exhumed subcontinental mantle rocks (Clerc & Lagabrielle, 2014; Lagabrielle & Bodinier 2008; Lagabrielle et al., 2010; Lagabrielle et al., 2016). The significance of subcontinental mantle rocks exposed here has led to models that invoke extreme crustal attenuation and mantle exhumation during the Early Cretaceous (e.g., Clerc et al., 2014; De Saint Blanquat et al., 1990; Fabriès et al., 1991; Jammes et al., 2009; Lagabrielle et al., 2010). Unlike many other inverted margins within mountain belts (e.g., Alpine tethyan rift margin), the thermal pattern and geometries of the fossil rift margin are not significantly overprinted because the Pyrenees never underwent oceanic subduction and there was limited shortening (~20 km) in the retro-wedge NPZ as most of the shortening and crustal overthrusting occurred south of the North Pyrenean Fault (Grool et al., 2018, and references within). The preservation of features associated with hyperextension including exhumed subcontinental mantle, deep crustal rocks (granulites), and HT-LP metamorphism of prerift and synrift deposits and the existence of upper crustal boudinage associated with the strong Early Cretaceous thermal anomaly (Clerc et al., 2016; Clerc & Lagabrielle, 2014; Corre et al., 2016; Hart et al., 2016; Masini et al., 2014; Teixell et al., 2016; Tugend et al., 2015; Vacherat et al., 2016) make the NPZ an analog suited to study distal margins and geodynamic processes associated with hyperextension at magma poor margins.

This study applies integrated multi-mineral U-Pb thermochronometry from the Agly Massif (Figure 1) to distinguish between Variscan and Early Cretaceous deformation and to elucidate the exhumation history and thermal processes in the continental crust associated with hyperextension and mantle exhumation at magma poor margins. The Agly Massif represents a condensed crustal section that has been previously interpreted as a rift block and/or a crustal boudin at the distal margin, allowing for direct sampling of upper and lower crustal rocks (Clerc & Lagabrielle, 2014; Vauchez, Clerc, et al., 2013).

While upper-crustal extension during initial stretching in proximal continental margins is well understood, the structural and thermal evolution of the middle and lower crust during decoupled and coupled hyperextension remain mainly model driven and poorly understood. Many rift models have hypothesized that the upper crust and lower crust become decoupled which allows the lower crust and mantle stretch more than the upper crust at the center of the rift (e.g., Brun & Beslier, 1996; Clerc et al., 2018; Lavier & Manatschal, 2006; Sutra & Manatschal, 2012; Driscoll & Karner, 1998; Whitmarsh et al., 2001). During decoupled extension crustal deformation is accommodated in the ductile layer of the crust, while during coupled extension, there is a transfer of brittle deformation to deeper crustal and mantle levels (e.g., Sutra & Manatschal, 2012). Different rift models predict different timing of coupling of the lower and upper crust, so constraining the timing of coupling is important for linking the geologic record with geodynamic models (e.g., Brun & Beslier, 1996; Driscoll & Karner, 1998; Whitmarsh et al., 2001).

The NPZ, including the Mauleon, the Ariege, and Agly areas, is regarded as one of the world's best examples of an exhumed fossil magma-poor hyperextended continental margins with limited orogenic overprinting of rift and thermal evolution and offers the possibility for direct observation and sampling (e.g., Clerc et al., 2014; Masini et al., 2014; Tugend et al., 2015). The Agly Massif has structural features including boudinage of the prerift sedimentary rocks (Clerc & Lagabrielle, 2014; Chelalou et al., 2016; Vauchez, Clerc, et al., 2013) and localization of deformation along ductile shear zones (Olivier et al., 2004) that are characteristic of rifting and passive margin formation. Similar structural features have been imaged in present-day rifted margins, including crustal boudinage, ductile shear and low-angle detachment faulting, and a Continent Dipping Normal Fault (CDNF). Medium- and high-temperature thermochronometric data provide an important puzzle piece in understanding the structural and thermal evolution of the middle and lower crust. In particular, the data alleviate ambiguities related to the timing of structures and differentiate between inherited prerift structures and shear zones that are active during rifting and contribute to the tectonic attenuation of the crust and thermal evolution of continental crust in the distal margin.

Rutile and apatite U-Pb thermochronometry has the potential to elucidate the precursor rift thermal history as they are less susceptible to overprinting by inversion and collisional tectonics than low-temperature thermochronometers. These techniques can be used to constrain the chronology of tectonic and thermal processes associated with hyperextension and subcontinental mantle exhumation in a fossilized distal margin. Some of the scientific community has considered ductile deformation in the North Pyrenean Massifs as being exclusively Variscan aged (e.g., Olivier et al., 2008, and references within), but high- and medium-temperature thermochronometers presented here have the power to identify the Cretaceous overprint. A better understanding of the Early Cretaceous preorogenic history of the margin also has major implications for understanding the effect of inherited rifted margin architecture on the evolution of the Pyrenean orogen (e.g., Mouthereau et al., 2014; Teixell et al., 2016; Vacherat et al., 2014; Velasque et al., 1989).

2. Geologic Setting

2.1. The Agly Massif

The NPZ is a narrow fold-thrust belt north of the North Pyrenean Fault (Figure 1) that preserves features from its Cretaceous preorogenic extensional history, including discontinuous Variscan basement massifs, bodies of subcontinental mantle, and middle to late Cretaceous inverted metamorphic basins (e.g., Jammes et al., 2009; Masini et al., 2014; Mouthereau et al., 2014; Vauchez, Clerc, et al., 2013). The NPZ basement massifs are variably interpreted as crustal blocks that have been ductiley thinned during (i) the Carboniferous associated with metamorphic doming (e.g., Olivier et al., 2004, 2008) or (ii) lithospheric thinning and exhumation of subcontinental mantle due to the Iberian microplate displacement relative to Eurasia in the Cretaceous (e.g., Clerc et al., 2014; Jammes et al., 2009; Masini et al., 2014; Paquet & Mansy, 1991)The Agly Massif is the easternmost basement massif within the NPZ. It represents a tilted ~10-km-thick condensed crustal section composed of Variscan HT-LP metamorphic (granulite to greenschist facies) and plutonic rocks (Barnolas et al., 1996; Guille et al., 2018; Olivier et al., 2008; Wickham & Oxburgh, 1986; Figure 1a). The upper part of the crustal section (surface to 12–14 km) is composed of Paleozoic metasedimentary strata and magmatic granitoids. The middle lower part (14- to

22-km depth) is composed of amphibolite and granulite facies paragneisses and orthogneisses that show evidence of high strain that has been attributed to deformation during the Variscan/Hercynian orogeny (e.g., Bouhallier et al., 1991; Olivier et al., 2004, 2008;Wickham & Oxburgh, 1986) or during the Cretaceous (Delay, 1990; Delay & Paquet, 1989; Paquet & Mansy, 1991). These prethinning depth estimates suggest that the Agly Massif has been thinned to about half its original thickness that had been acquired by the end of the Variscan orogeny (~20–22 km) to its present-day thickness of ~8–10 km.

The Agly Massif is divided into two domains based on lithology: a northeast domain and a southwest domain. The northeast domain is composed of northeast to east gently dipping Cambrian-Ordovician metapelites where the low-pressure metamorphism increases down section (toward the SW) from greenschist facies (~350 °C, <200 MPa) to upper amphibolite facies conditions (600–650 °C, <400 Mpa; Vauchez, Clerc, et al., 2013). The southwest domain is composed of high-grade gneisses and magmatic intrusives with the highest-grade rocks being anatectic granulites and charnockites near southern border of the massif. This study focuses mainly on the southwest domain of the massif where the oldest and highest-grade metamorphic rocks outcrop in the southern part of the massif (Figure 1b).

The Saint-Arnac pluton, the northwest part of the Agly massif (Figure 1), was emplaced into Cambro-Ordovician metapelites during the Carboniferous Variscan orogeny. The central and northern parts of the pluton are composed of monzogranites with crystallization pressure estimates in the north of 1–1.5 kbar (Olivier et al., 2008). The southern part of the pluton is formed by granodiorites and tonalities in the west and granodiorites and diorites in the east with P-T conditions (based on country rock assemblages) estimated at 2.5–3 kbar and 650–700 °C (Vielzeuf, 1996). The metamorphic grade of the country rock that the pluton intruded increases to the south (from greenschist facies to sillimanite bearing micaschists) indicating that the southern boundary observed today corresponds to the floor of the pluton, and the northern part is close to the roof of the pluton (Olivier et al., 2004). These relationships indicate that the pluton was emplaced at a depth of 10 km to less than 5 km and has been tilted northward since emplacement (Clerc & Lagabrielle, 2014; Olivier et al., 2008). The observed thickness of the pluton is ~5 km from the floor to the highest exposure in the north. Previous studies have dated crystallization ages for the Saint Arnac pluton using zircon U-Pb geochronology 308.3 ± 1.2 Ma and 306.6 ± 4.7 Ma (Olivier et al., 2008) and 293 ± 23 Ma (Poujol et al., 2010). Monazites from Lansac albitites were dated at 98 ± 2 Ma, interpreted to date the albitization of the pluton (Poujol et al., 2010).

Below the pluton to the south is an orthogneissic band, the Riverole Gneiss, that was at an initial depth of 12–15 km during the emplacement of the Saint Arnac pluton during the late Variscan times (Olivier et al., 2008). It has been interpreted as belonging to the SW floor of the pluton (Fonteilles, 1976) and is presently located near a high-temperature mylonitic normal shear zone at the base of the Saint-Arnac pluton (Olivier et al., 2008).

The highest-grade rocks in the massif are anatectic granulites and charnockites in the southern part of the massif. The Caramany gneisses, hyperstene, and hyperstene + hornblende are the deepest rocks exposed, with the Bélesta Gneiss, cummingtonite, and sillimanite+K-spar zones, above (Olivier et al., 2004). The Ansignan charnockite is an ~1-km-thick laccolith that was at P-T conditions; temperatures are estimated around 650–800 °C for pressures of around 3.5 to 6 kbar (Andrieux, 1982a, 1982b; Barbosa & Fonteilles, 1986; Vielzeuf, 1984) and an estimated depth of ~18 km during emplacement at 314 ± 6 Ma (Respaut & Lancelot, 1983) at the base of the Caramany gneisses (Olivier et al., 2008). There is a 1-km-thick band of Bélesta gneiss with P-T conditions of metamorphism estimated at 3.5–4 kbar and 650–700 °C (Vielzeuf, 1984; Guille et al., 2018) between the Ansignan charnockitic granite and the Saint-Arnac pluton. The gneiss is bounded by the Rentadou fault to the north and Ansignan fault to the south (Figure 1).

The timing of crustal thinning and mylonitization and origin of the present-day apparent geothermal gradient, locally up to 100 °C/km (Delay, 1990; Fonteilles, 1976; Olivier et al., 2004; Vielzeuf, 1984), is still debated. Previous models have interpreted thinning as resulting from (i) late to post-Variscan crustal thinning along a northward detachment (Bouhallier et al., 1991), (ii) local thinning on the limbs and roof during doming related to dextral transpression or regional change to extensional stress regime after Carboniferous dome formation (Olivier et al., 2004, 2008), and (iii) Cretaceous crustal thinning along a deep northward detachment (Delay, 1990; Delay & Paquet, 1989; Paquet & Mansy, 1991).

2.2. Basins in the Agly Region

The massif is surrounded by three E-W trending synclines composed of Triassic, Jurassic, and Cretaceous (up to Cenomaniam) sedimentary strata: the Boucheville syncline to the south, Lower Agly syncline to the NE, and the St-Paul de Fenouillet syncline to the North (Figure 1b). The Boucheville syncline is composed of metamorphosed Aptian to lower Cenomanian "flysch noir" deposited as the basin opened in relation to Albian extension (Chelalou et al., 2016). These sedimentary strata were metamorphosed at temperatures of 530–580 °C dated at circa 97 Ma using in situ laser ablation inductively coupled plasma mass spectrometry (LA-ICP-MS) U-Pb dating of titanite grains found in syndeformational mineralization located in the Albian calcschists, providing constraint for both the deformation and metamorphism (Chelalou et al., 2016). The contact between Variscan granulites and charnockites of the Agly massif with Aptian-Albian flysch is a major subvertical fault which has been interpreted as an extensional fault that formed in relation to Boucheville basin opening (Figure 1) that shows evidence of reactivation and reverse movement (Chelalou et al., 2016; Vauchez, Clerc, et al., 2013). The sedimentary strata in the Bas-Agly syncline are partially metamorphosed with temperature estimates ~350–500 °C, and sedimentary strata of the Saint-Paul-de-Fenouillet syncline have the lowest temperature metamorphism with temperatures <200 to 300 °C (Chelalou et al., 2016; Golberg & Leyreloup, 1990). The northeast contact between basement and cover in the Lower Agly syncline has limited Pyrenean orogenic imprint with the schistosity with sedimentary strata concordant with metapelites. However, the northwest contact was more affected by Pyrenean orogenic overprint making the relationship between basement and its Mesozoic cover difficult to interpret (Vauchez, Clerc, et al., 2013). No clasts from the Agly Massif basement units have been found in Aptian-Lower Cenomanian sedimentary strata, suggesting that neither the sedimentary cover nor basement was significantly eroded before the Late Cretaceous (Vauchez, Chauvet, et al., 2013).

2.3. Previous Age Constraints/Geochronology

Numerous studies have performed geochronologic analyses on the Agly Massif and surrounding areas and provide important constraints on the understanding of the preorogenic evolution. Different phases within the Saint Arnac pluton have been dated by zircon U-Pb geochronology using conventional isotope dilution thermal ionization mass spectrometry techniques, yielding ages of 303.6 ± 4.7 for Saint Arnac pluton (Olivier et al., 2004), 307 ± 0.4 for a deformed granite at base of Saint Arnac pluton, 314.2 ± 0.9 Ma for a granodiorite, and 308.3 ± 1.2 Ma for the Tournefort diorite, at the SW corner of the Saint Arnac pluton (Olivier et al., 2008). Zircon U-Pb geochronology yielded an age of 314 ± 6 Ma for the Ansignan charnockite (Respaut & Lancelot, 1983), 315 ± 5 Ma (Postaire, 1984) and 307 ± 3 (Guille et al., 2018) for the charnockite pluton, and 295 + 5/−3 Ma for the garnet leptynite (Respaut & Lancelot, 1983). The deformed deep-seated monzogranite in Bélesta gneiss was dated using zircon U-Pb at 317 ± 3 Ma (Olivier et al., 2004) and 307 ± 3 to 298 ± 3 Ma (Guille et al., 2018). The orthogneiss sills that make up the majority of the Bélesta Gneiss unit were dated at 542 ± 4 and 540 ± 2 Ma (Guille et al., 2018). The paragneisses that make up the majority of Caramany Gneiss unit have zircon U-Pb ages of 299 ± 4 Ma reflecting migmatization ages, with sills of orthogneiss dated at 529 ± 5 Ma and sills of granodiorites dated at 308 ± 3 to 299 ± 3 Ma (Guille et al., 2018). Biotite Rb-Sr (T_c = 300–380 °C) dating from granulite and granite gave ages of 100–130 Ma (Roubault et al., 1963). Albitization/metasomatism of the Agly Massif in the Lansac area (Figure 1) was dated using U-Th-Pb on monazite at 98 ± 2 Ma (Poujol et al., 2010) and of the Salvezines Massif, the NPZ basement massif ~5 km to the west from the Agly Massif, using muscovite $^{40}Ar/^{39}Ar$ at 117.5 ± 0.4 Ma (Boulvais et al., 2007). Mylonitization in the Millas granite, to the south in the Axial Zone (Figure 1), was interpreted to be 90–100 Ma using biotite, muscovite, and K-spar $^{40}Ar/^{39}Ar$ data (Monie et al., 1994). HT-LP metamorphism of the Mesozoic cover, hydrothermal alteration, and alkaline magmatism in the NPZ have been consistently dated between 110 and 85 Ma and attributed to Cretaceous rifting and hyperextension (Albarède & Michard-Vitrac, 1978; Boulvais et al., 2006, 2007; Clerc & Lagabrielle, 2014; Clerc, Lahfid, et al., 2015; Corre et al., 2016; Dauteuil & Ricou, 1989; Fallourd et al., 2014; Golberg et al., 1986; Golberg & Leyreloup, 1990; Hart et al., 2016; Montigny et al., 1986; Poujol et al., 2010).

Despite these timing constraints, differentiating between the Variscan and Cretaceous deformation and deciphering the Cretaceous rift thermal structure and potential Cretaceous reheating versus conductive cooling during exhumation remain debated. Novel analytical approaches of U-Pb zircon and apatite geochronometry and thermochronometry applied systematically across the basement massif and integration

with previous work offer the potential of resolving both the preorogenic Variscan and Cretaceous extensional thermal and exhumation history of the massif and can shed light on important thermal processes during hyperextension and continental break-up.

3. U-Pb and Trace Element Methodology

Twelve samples were collected from the massif along two roughly south to north, deepest to shallowest crustal levels, transects across the Caramany, Bélesta, and Riverole gneisses, the Ansignan charnockite, the Saint Arnac pluton, and Cambro-Ordovician metasedimentary strata (Figure 1). Samples were separated for zircon, apatite, and rutile using standard crushing, grinding, heavy-liquid, and magnetic separation techniques.

Samples are grouped according to their interpreted structural position prior to crustal thinning based on lithology, metamorphic grade, and/or crystallization or metamorphism P-T conditions into upper, middle, and middle-lower crustal samples. The upper crustal samples are from the Saint Arnac pluton (samples 15-AG-08, 17-AG-105, and 17-AG-106) that was intruded at depths of 10 to <5 km (Olivier et al., 2008) and the Cambro-Ordovician metasediments (sample 15-AG-01). The upper-middle crustal samples are from the Riverole Gneiss (samples 15-AG-07 and 17-AG-104). The middle-lower crust samples are from the Bélesta Gneiss, Caramany Gneiss, and the Ansignan charnockite (samples 15-AG-02, 15-AG-03, 15-AG-04, 15-AG-05, 15-AG-06, and17-AG-103), with an initial emplacement depth of ~20–22 km for the Ansignan charnockite (Andrieux, 1982a, 1982ab; Olivier et al., 2008; Vielzeuf, 1984, 1996).

In this study, multiple geochronometers and thermochronometers were employed to constrain the structural and thermal evolution of both the upper and middle crustal rocks of the Agly Massif. Zircon U-Pb ages record either the magmatic crystallization age of the rock or high-temperature metamorphism (Dahl, 1997; Schoene, 2014). The rutile U-Pb closure temperature is ~500 °C (Cherniak, 2000; Vry & Baker, 2006), and apatite U-Pb closure temperature is ~425–550 °C (Chamberlain & Bowring, 2001; Schoene & Bowring, 2007) making these minerals powerful for constraining cooling and exhumation histories of the middle and lower crust.

All mineral separation and LA-ICP-MS analyses were completed at the UTChron facilities at the Jackson School of Geosciences at the University of Texas at Austin.

3.1. Zircon U-Pb Methodology

Zircon grains were picked from the nonmagnetic heavy mineral separate using an optical microscope and mounted onto double-sided tape on 1-in. acrylic mounts and analyzed using LA-ICP-MS U-Pb depth profiling, following procedures described in Marsh and Stockli (2015) and Hart et al. (2016). For depth profile analysis, zircons were ablated with a 30-μm spot size using a PhotonMachine Analyte G.2 193-nm Excimer Laser for 30 s at 10 Hz. GJ1 was used as the primary zircon standard (601.7 ± 1.3 Ma; Jackson et al., 2004) and Pak-1 (43.03 ± 0.01 Ma; in-house standard dated by thermal ionization mass spectrometry (TIMS)), 91500 (1065 Ma Wiedenbeck et al., 1995), and Plesovice (337.13 ± 0.37 Ma TIMS; Sláma et al., 2008) as secondary standards. At least 30 grains were analyzed for magmatic and metamorphic rocks, and 120 grains were analyzed for detrital samples. Time and depth-resolved data reduction was performed using Iolite software with the IgorPro (Paton et al., 2011) and VisualAge data reduction scheme (Petrus & Kamber, 2012). Data were visualized using IsoPlot (Ludwig, 2012). All reported uncertainties are 2σ and all analytical data and methodologic procedures are detailed in supporting information.

3.2. Rutile U-Pb and Trace Element Methodology

Rutile grains were handpicked from the bulk heavy mineral separate, mounted in epoxy, and polished for grain-internal LA-ICP-MS U-Pb analysis. Rutile grains were analyzed using the same ablation settings, with a 40-μm spot size, and ICP-MS data acquisition parameters as used for zircon U-Pb. Rutile R10 (1090 ± 0.9 Ma; Luvizotto et al., 2009) was used as a primary reference standard and rutile R19 (489.5 ± 0.9 Ma; Zack et al., 2011) as a secondary reference standard. Analysis and data reduction were done following methodology of Smye and Stockli (2014). Data reduction was also performed using Iolite data reduction software and VisualAge data reduction scheme (Petrus & Kamber, 2012).

Selected trace elements (Al, Ca, Ti, V, Cr, Fe, Zr, Nb, M, Sn, Sb, Hf, Ta, W, and U) were measured by LA-ICP-MS following the methodology outlined by Smye and Stockli (2014) to determine petrotectonic affinity and crystallization temperatures of rutile. Zr-in-rutile crystallization temperatures were calculated using the calibration of Tomkins et al. (2007). A 40-μm spot size was used for trace element LA-ICP-MS determinations, and concentrations were calibrated against SRM 610 (NIST) reference glass standard. Data reduction was also performed using Iolite data reduction software and Trace Element_IS (Paton et al., 2011).

3.3. Apatite U-Pb Methodology

Apatite grains were picked using an optical microscope and mounted onto double-sided tape on 1-in. acrylic mounts and analyzed using LA-ICP-MS U-Pb depth profile dating. The apatite U-Pb depth profile analyses were completed using a PhotonMachine Analyte G.2 Excimer laser with a large-volume Helex sample cell and a Thermo Element2 ICP-MS. MAD apatite (Thomson et al., 2012) was used as the primary reference standard (in-house TIMS ages of 472.4 ± 0.7 Ma) and UWA-1 (TIMS ages of 1010.8 ± 5 Ma; in-house standard) and McClure Mountain (523.5 ± 1.5 Ma; Schoene & Bowring, 2006) as secondary reference standards. A 40-μm laser spot was used to ablate ~18–20 μm deep (30 s at 10 Hz) on the prism plane of unpolished apatite, yielding a depth profile for each analyzed apatite. Ablation rates and pit depths were determined using a Bruker Contour GT-K1 3-D surface profilometer in VSI mode with a nominal depth precision of ±<1 nm. Data from the analyses were reduced using Iolite data reduction software and VizualAge_UcomPbine (Chew et al., 2014).

U-Pb results were calculated from multiple apatite whole-grain (bulk) integrations and depth profiles for individual apatite grains. Bulk sample Tera-Wasserburg concordia intercept ages were calculated from arrays of whole-grain/bulk sample apatite data, forming common Pb (Pb_c) and radiogenic Pb (Pb*) mixing line discordia arrays (Tera & Wasserburg, 1972). Tera-Wasserburg Concordia diagrams and age profile plots were made using Isoplot 4.15 (Ludwig, 2012).

For individual apatite grain depth profiles, the continuous ablation signal traces were divided into 3.1-s ablation time(~1.5-μm) depth increments. The 14 increments were plotted on Tera-Wasserburg Concordia diagrams and used to calculate lower and upper intercepts for single apatite grains. An intra-grain 207Pb correction was applied to the 3-second integration increment age using the Pbc upper intercept value from the discordia line in Tera-Wasserberg Concordia space (e.g. Boyd et al., 2017). This technique enables the resolution and visualization of the U-Pb age to elucidate the intragrain U-Pb systematics and the interpretation of bulk apatite U-Pb ages. Intragrain apatite U-Pb increments were plotted as age spectra similar to data using Isoplot (Ludwig, 2012). Individual age spectra were stacked to examine overall U-Pb topology within samples and to evaluate the thermal history of samples (Seymour et al., 2016).

4. Results

Zircon, apatite, and rutile U-Pb and trace element results are grouped into upper, upper-middle, and middle-lower crust based on previous geological and P-T constraints (i.e., Andrieux, 1982a, 1982ab; Clerc & Lagabrielle, 2014; Guille et al., 2018; Olivier et al., 2004, 2008; Respaut & Lancelot, 1983; Wickham & Oxburgh, 1986). The upper crust consists of the Paleozoic metasedimentary rocks and the Saint Arnac pluton, the upper-middle crust consists of the Riverole Gneiss, and the middle-lower crust consists of the Caramany and Bélesta Gneisses and Ansignan charnockite. Zircon U-Pb results are represented and summarized as Wetherill concordia diagrams, $^{206}Pb/^{238}U$-Pb weighted mean diagrams, and Kernel Density Estimate (Vermeesch, 2012) plots in Figures 2 and 3 and tabulated in the supporting information (S2). For crystalline basement samples, only zircon analyses with discordance <5% were used for age determinations. Weighted mean $^{206}Pb/^{238}U$-Pb ages for the youngest mode (excluding inherited age components) were calculated using the TuffZirc approach (Ludwig & Mundil, 2002). The algorithm extracts the youngest coherent age component from complex single-zircon age distributions, attempting to account for inheritance and Pb loss.

Rutile U-Pb data for a single rutile-bearing sample from the Caramany Gneiss are displayed as both Tera-Wasserburg concordia diagram with a lower intercept age and ^{208}Pb-corrected weighted mean $^{206}Pb/^{238}U$-Pb age diagram (Figure 4). Apatite U-Pb age results are presented as multigrain bulk Tera-Wasserburg

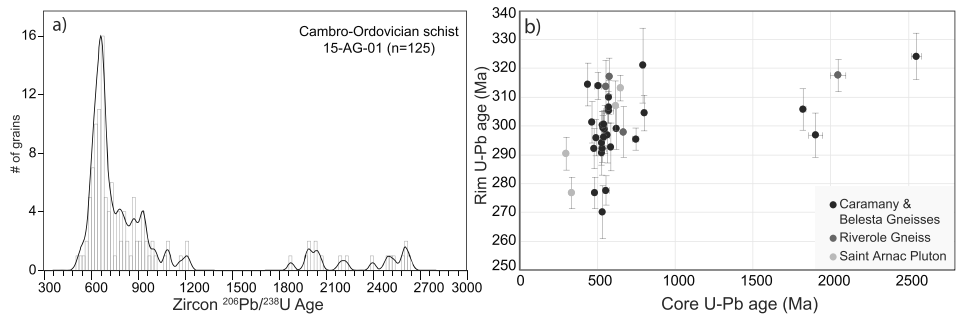

Figure 2. (a) KDE of detrital zircon U-Pb ages from Cambro-Ordovician metasediments (binwidth and bandwidth = 20 Myr). (b) Zircon rim versus core ages grouped by lithologic unit.

concordia diagrams (Figure 5) with regressed lower intercept ages. In addition, incremental apatite intragrain U-Pb ages are presented as age spectra (Figure 6).

4.1. Upper Crust: Cambro-Ordovician Schists and Saint Arnac Pluton

Sample 15-AG-01 from Cambro-Ordovician metasedimentary unit that never exceeded greenschist-facies conditions has a detrital zircon distribution (n = 121) with a major age component of ~650 Ma (47.5%) and minor components of ~ 500, ~800, ~950, ~1100, ~1900, and ~2400 Ma (1.7%, 20.8%, 10%, 6.7%, 5.8%, and 7.5%, respectively; Figure 2).

All three samples analyzed from the Saint Arnac pluton are granodiorites. The three samples from the Saint Arnac pluton, 15-AG-08, 17-AG-105, and 17-AG-106, have calculated ages of 301.0 + 2.8/−1.8 Ma (n = 26 of 38), 308.0 + 3.6/−2.2 Ma (n = 21/30), and 309.4 ± 2.2 Ma (n = 21/36). There are rare xenocrystic zircons of Ordovician (n = 1) and Neoproterozoic age (n = 5). The grouped samples have a calculated age of 306.1 + 0.9/−1.9 Ma (n = 55/104; Figure 3).

All three samples from the Saint Arnac pluton have apatite U-Pb ages that are within error of their zircon U-Pb age. Sample 17-AG-105 has an age of 304 ± 15 (n = 48) and MSWD (mean square weighted deviation) of 16. The bulk sample age for 17-AG-106 is 331 ± 30 (n = 23) with a MSWD of 5.2. The bulk sample age for 15-AG-08 is 319 ± 13 (n = 20) with MSWD of 4.7. Since these ages are slightly older (though within error) of the zircon U-Pb ages with large errors, all the 3-s integration data for each sample excluding grains with low radiogenic Pb (excluded integrations with $^{206}Pb/^{238}U$ uncertainty >0.6 and excluded integrations with $^{238}U/^{206}Pb < 8$) were plotted with ages calculated to minimize common or inherited Pb from the age calculations. With these 3-s integrations excluded, 15-AG-08 has an age of 304.4 ± 3.1 Ma (n = 79) and MSWD of 4.0 and sample 17-AG-106 has an age of 312.6 ± 2.3 Ma (n = 262) with an MSWD of 3.1 (3-s data, gray ellipses in Figure 5). The single grain age versus depth profile for sample 17-AG-105 (Figure 6) shows a relatively flat age spectrum with single grain plateau ages overlapping with the whole sample Tera-Wasserburg bulk apatite ages and with the zircon U-Pb age.

4.2. Upper-Middle Crust: Riverole Gneiss

The two samples from the Riverole Gneiss show two main components of zircon single grain ages, one Ordovician (~450 Ma) and one Carboniferous-earliest Permian (~300 Ma) (Figure 3). The Carboniferous-Permian component in sample 15-AG-07 has a calculated 307.0 + 6.5/−6.1 Ma (n = 13/17), where 13 of the 17 ages in this range are zircon rim ages (12/13 used in TuffZirc calculation). The Ordovician component in sample 15-AG-07 has a calculated age of 451.4 + 4.7/−4.0 Ma (n = 21/28), where 11 of the ages in this range are zircon core ages (10/11 used in calculation). The Carboniferous-Permian component in sample 17-AG-104 has a calculated age of 312.9 + 4.4/−3.9 Ma (n = 12/15), where four of these ages are zircon rim ages. There are also grains with Ordovician ages (n = 4) and zircon cores of Cambrian (n = 1) and Neoproterozoic (n = 4) ages (Figure 2). A mean age for the Carboniferous component has been calculated for the two samples at 310 + 3.5/−7.5 Ma (n = 21/34; Figure 3).

Sample 15-AG-07 has an apatite U-Pb lower intercept age of 153 ± 36 (n = 13; Figure 5). Many of the analyses had large error correlations, and analyses with an internal $^{206}Pb/^{238}U$ standard error > 0.005 are rejected

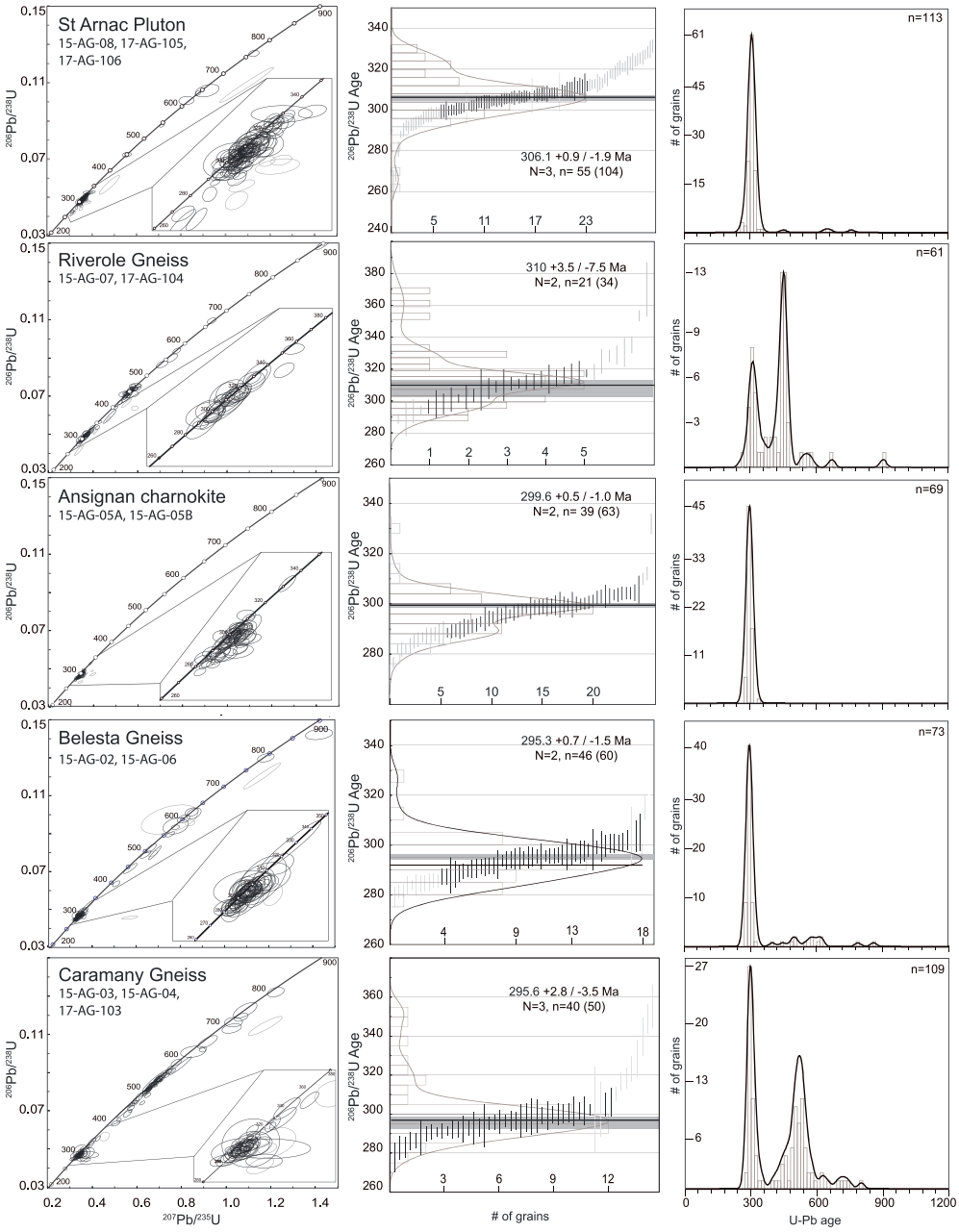

Figure 3. Zircon U-Pb results, grouped by lithologic unit. (left column) Wetherill Concordia diagrams, with inset showing larger-scale Concordia of the Variscan-aged grains. Ellipses in black are <5% discordant, and ellipses in gray are 5–10% discordant. (middle column) Plots showing the Variscan component in each sample used to calculate ages with TuffZirc with each bar representing one zircon $^{206}Pb/^{238}U$ age (data shown in gray excluded from calculations), with the calculated $^{206}Pb/^{238}U$ age and error represented as the horizontal line and gray box. Kernel Density Estimation plots with histograms are overlain to show the age distributions. Right column: Kernel Density Estimation plot of all analyzed zircons from each unit, with histograms (binwidth and bandwidth = 20 Myr).

(large errors). Sample 17-AG-104 has a lower intercept age of 267 ± 20 (n = 41; Figure 5). The single grain age versus depth profile for sample 15-AG-07 (Figure 6) shows a wide scatter of age ranges that fall between ~450 and ~100 Ma. The topologies of single grains are highly variable. A subset of the analyzed apatite grains was picked from the tape mount, rotated 90°, mounted in epoxy, and polished to expose a cross section of the laser ablation pit to look at potential zoning patterns associated with the potential crack and seal deformation and apatite growth. Apatite shows obvious zoning or recrystallization along the margins as

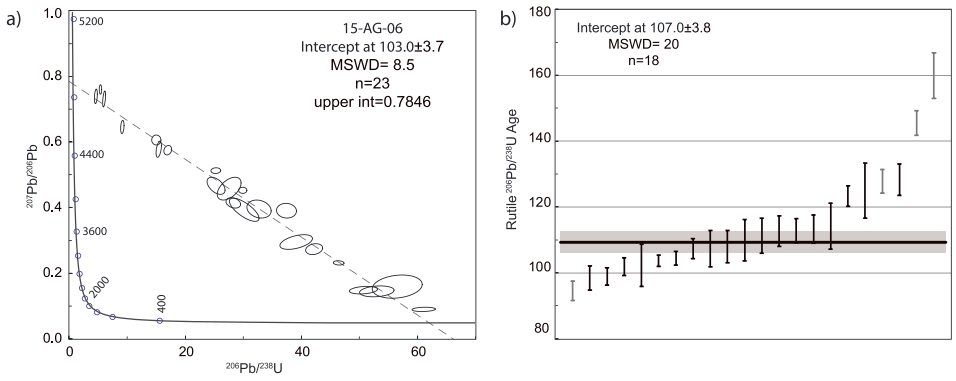

Figure 4. Rutile U-Pb results. (a) Rutile U-Pb Terra-Wasserburg Concordia plots. Uncertainties are 2σ. (b) Weighted mean average of single grain Pb_c corrected $^{206}Pb/^{238}U$ ages.

well as along intragrain cracks in backscatter electron and cathodoluminescence image analysis supporting the observed complex age versus depth profiles (supporting information Figure S1).

4.3. Middle-Lower Crust: Caramany Gneiss, Bélesta Gneiss, and Ansignan Charnockite

The two samples from the Ansignan charnockite, 15-AG-05A (porphyritic granodiorite) and 15-AG-05B (garnet orthopyroxene-bearing leucogranite), have calculated zircon U-Pb ages of 288.5 + 2.7/−1.2 Ma (n = 19/36) and 299.1 + 3.9/−1.4 Ma (n = 22/27). The grouped samples have a calculated age of 299.6 + 0.5/−1.0 Ma (n = 39/63). The Bélesta Gneiss and samples 15-AG-02 and 15-AG-06 have a calculated age of 295.3 + 4.2/−1.9 Ma (n = 24/36) and 295.5 + 1.7/−4.0 Ma (n = 21/24), respectively, with a calculated group age of 295.3 + 0.7/−1.5 Ma. There are single grains and grain cores of Cambrian (n = 2) and Neoproterozoic (n = 9) ages (Figures 6 and 2b).

The three samples from the Caramany Gneiss show two main components of zircon single grain ages, one Cambrian (~530 Ma) and one Carboniferous-earliest Permian (~300 Ma; Figure 3). The Carboniferous-Permian component in sample 15-AG-03 has a calculated 291.0 + 5.4/−3.5 Ma (n = 8/9), where 13 of the 17 ages in this range are grain rim ages (12/13 used in calculation). The Cambrian component in sample 15-AG-03 has a calculated age of 503.2 + 4.0/−7.2 Ma (n = 14/20), where five of the ages in this range are core ages (3/5 used in calculation). The Carboniferous-Permian component in sample 15-AG-04 has a calculated age of 293.5 + 4.9/−1.5 Ma (n = 20/25), where four of these ages are grain rim ages. There are also grains and grain cores of Ordovician (n = 4) and Cambrian (n = 4) ages (Figures 6 and 2b). The Carboniferous-Permian component in sample 17-AG-103 has a calculated 299.8 + 4.8/−3.7 Ma (n = 12/13), where 10 of the 12 ages in this range are grain rim ages. The Cambrian component in sample 15-AG-03 has a calculated age of 532.5 + 3.1/−12.1 Ma (n = 6/9), where two of the ages in this range are core ages. There are single grains and grain cores of Neoproterozoic (n = 19) ages. The mean age for the Carbonifeous components from the three samples was calculated at 295.0 + 1.4/−2.0 Ma (Figure 3).

All samples from the middle-lower crust have Aptian apatite U-Pb ages (Figures 4 and 7). Sample 15-AG-03 has an age of 113.5 ± 4.3 Ma (n = 44). Sample 15-AG-05A has an age of 119.6 ± 6.8 (n = 19). Sample 15-AG-06 has an age of 119 ± 18 Ma (n = 39). Sample 17-AG-103 has an age of 127 ± 16 Ma (n = 9). Sample 15-AG-01 has an age of 115.8 ± 7.9 Ma (n = 32). The stacked single grain age versus depth profiles for sample 15-AG-03 (Figure 6) show a flat profile with the single grain profiles overlapping with the whole sample apatite Tera-Wasserburg age but much younger than the Permian zircon U-Pb rim age.

Rutile was only found in one sample from the Bélesta Gneiss (15-AG-06). Rutile U-Pb and trace element analysis were performed on polished rutile grains and ages corrected using the methods of Zack et al. (2011). The weighted mean average of single grain ages is age is 107.0 ± 3.8 Ma, and the lower intercept age on a Tera-Wasserburg is 103.0 ± 3.7 (MSWD = 8.5). The Zr-in-rutile thermometer (Zack et al., 2013) gives temperatures ranging from 757 to 590 °C with a mean of 657 °C. The Zr-in-rutile thermometer that yields crystallization temperatures is consistent with previous thermometry estimates for the Bélesta Gneiss (Vielzeuf, 1984). The [Cr] and [Nb] based classification scheme of Triebold et al. (2012) indicated that all but two rutile grains are metafelsic.

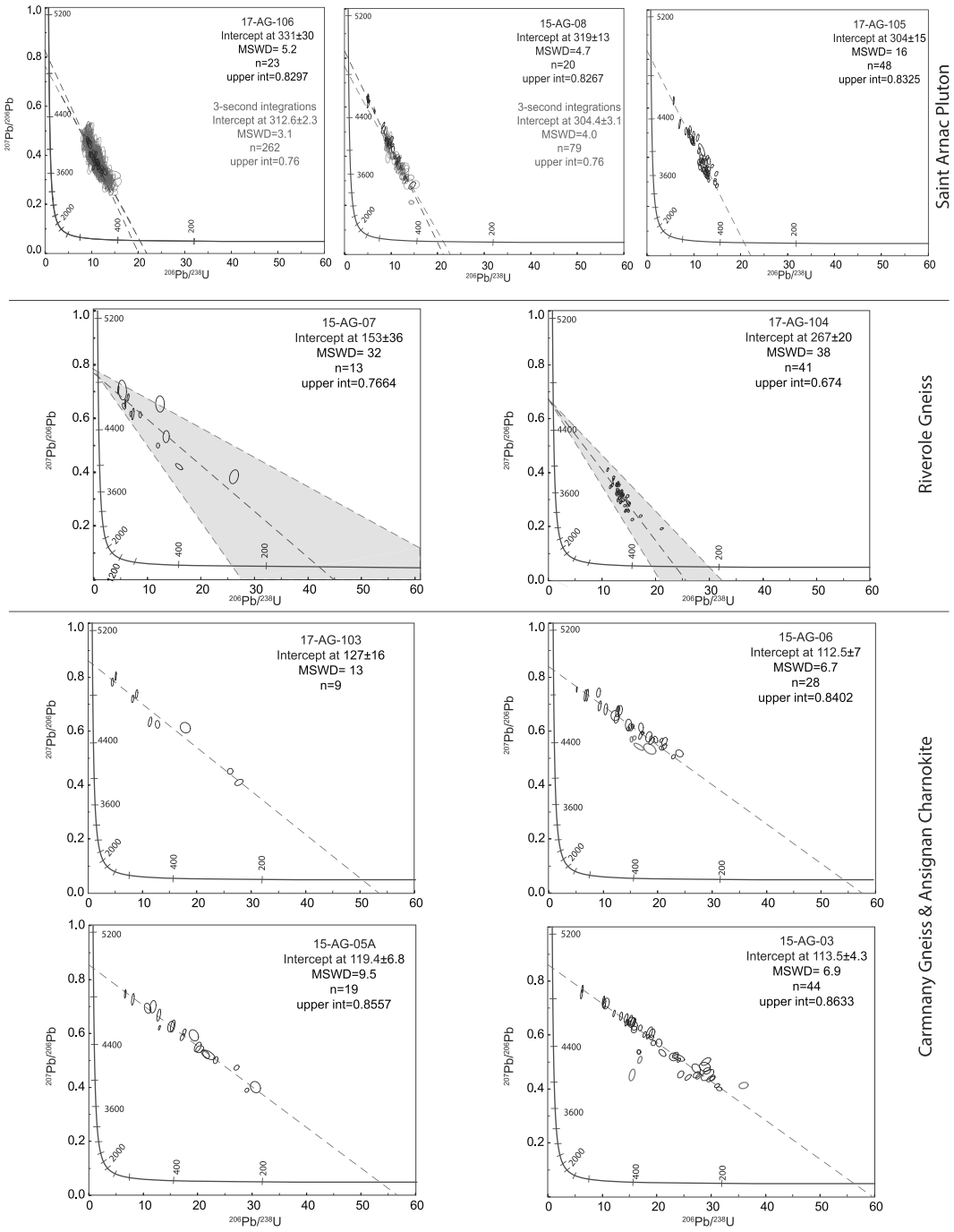

Figure 5. Apatite U-Pb Tera-Wasserburg plots. Uncertainties are 2σ.

5. Discussion

New high-temperature thermochonometric data add new constraints on the preorogenic evolution of the Agly Massif in the eastern Iberia-European margin. The data clearly indicate rapid exhumation and cooling of the middle to lower crust beginning in the Aptian (~120 Ma), predating regional HT metamorphism, mantle exhumation, metasomatism, and magmatism (~110–85 Ma). This provides key chronological constraints on the timing of crustal thinning in the Agly Massif and evolution of rifting and hyperextension processes

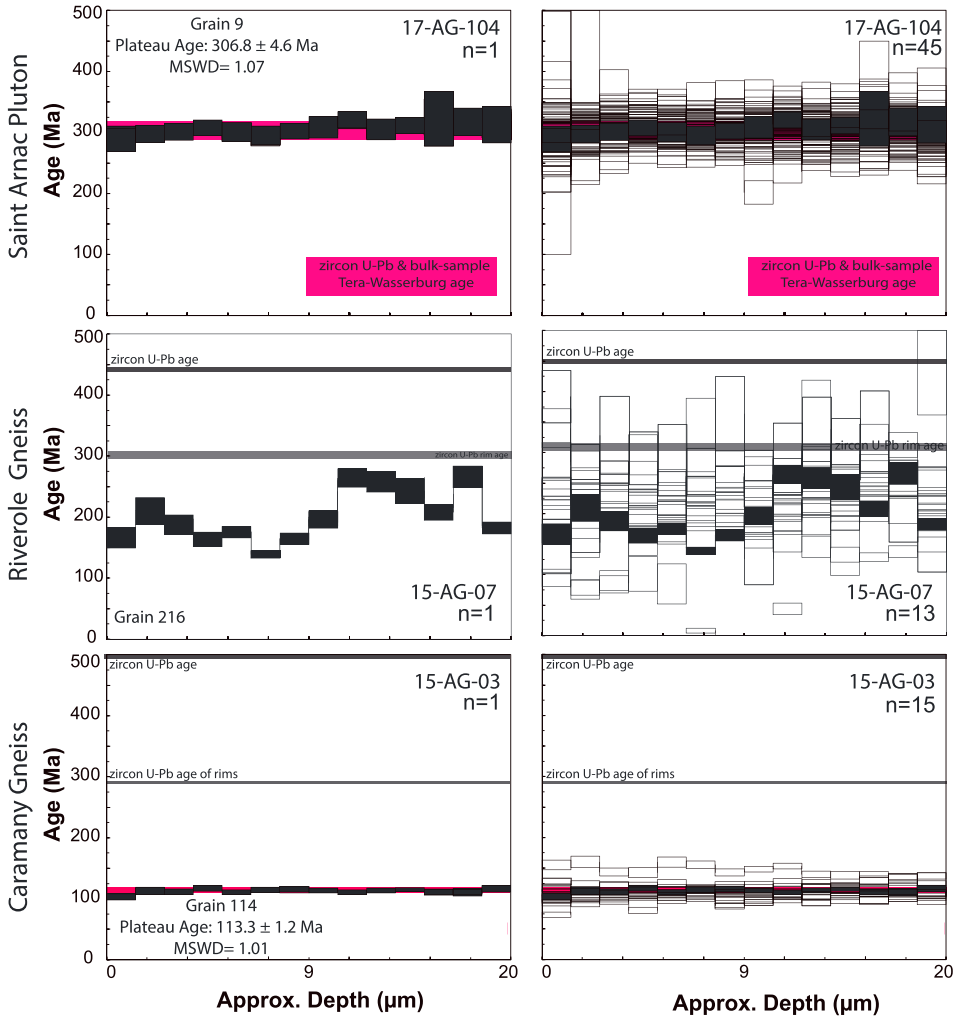

Figure 6. Apatite single grain U-Pb age spectra. (left column) One grain's age spectra. (right side) Stacked age spectra of all analyzed grains.

and allows for discriminating between proposed tectonic models of hyperextension for the eastern NPZ. In the following discussion, the new geochronological and thermochronological data are used to constrain the history of the massif from the magmatism associated with the Variscan orogeny through the onset of Pyrenean shortening, with the most important new constraints on the preorogenic hyperextension of the European margin in the present-day eastern NPZ.

5.1. Variscan Magmatic and Metamorphic Evolution

The zircon U-Pb data record the complex history of Paleozoic magmatism and metamorphism in the Pyrenean domain, related to Ediacaran- lower Cambrian (580–550 Ma) Cadomian magmatism, Ordovician (490–430 Ma) magmatism, and Variscan (350–280 Ma) orogeny and magmatism (Casas et al., 2010, and references within; Deloule et al., 2002; Mezger & Gerdes, 2016; Olivier et al., 2008; Paquet et al., 1997).

The Cambro-Ordovician metasedimentary sample (15-AG-01) has a detrital spectrum with a dominant component of Neoproterozoic (~600 Ma) aged grains, interpreted as Pan-African zircons, suggesting a dominant Gondwanan sediment source for the sedimentary protolith. The age spectrum is similar to those found in Cambro-Ordovician rocks in the Andorran Axial Zone (Margalef et al., 2016), Sardinia (Avigad et al., 2012), and Silicy (Williams et al., 2012) suggesting that these areas shared source areas in the Saharan Metacraton on the northeastern Gondwanan margin (Casas & Murphy, 2018; Margalef et al., 2016).

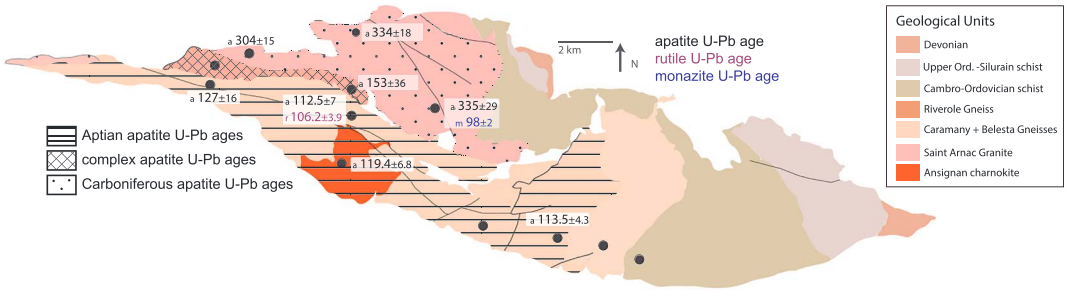

Figure 7. Map showing the spatial distribution of apatite U-Pb cooling ages, rutile U-Pb age, and monazite U-Pb age (from Poujol et al., 2010) throughout the massif. Massif map modified after Olivier et al. (2004).

The Saint Arnac granodiorite pluton samples, along with previously published ages (Olivier et al., 2004, 2008), indicate a period of emplacement between ~310 and 300 Ma in the upper crust synchronous with the late deformation phase of the Variscan orogeny (Aguilar et al., 2014). The emplacement ages do not show any correlation with either bulk rock composition (e.g., granodiorite versus tonalite) or relative crustal level. The Saint Arnac pluton is associated with the widespread calc-alkaline plutonism in the Pyrenees and neighboring areas (e.g., Catalan Coastal Ranges and Iberian Massif). The apatite U-Pb ages from the Saint Arnac pluton overlap the zircon U-Pb crystallization mean ages within error indicating the pluton was intruded and crystallized in the upper crust (<10-km depth; Olivier et al., 2008; Oosthuyzen & Burger, 1973) and never reheated to >450 °C (T_c apatite U-Pb).

The protoliths of the Caramany and Riverole Gneisses record two Ordovician magmatic events that were then metamorphosed during the Carboniferous-Permian Variscan orogeny. The Caramany Gneiss is dominated by Late Cambrian-Early Ordovician zircon U-Pb ages that record the emplacement of the gneiss protolith in the Early Ordovician—a period that gave rise to a number of large gneissic bodies in the core of the Eastern Pyrenean massifs Casas et al., 2010; Deloule et al., 2002, and references within). The Riverole Gneiss is characterized by Late Ordovician zircon U-Pb ages, recording protolith emplacement during a second magmatic event in the Late Ordovician. The Carboniferous-Permian rims on many zircons from the gneisses record high-temperature metamorphism and zircon crystallization during the late Variscan orogeny.

The Ansignan charnockitic samples have a crystallization age of 299.6 + 0.5/−1 Ma. This is consistent with a previously published age of 295 + 5/−3 Ma for the garnet leptynite near the contact between the Caramany Gneiss and Ansignan charnokite, which is interpreted as a melting product of the surrounding gneiss during emplacement of the Ansignan chanockite pluton (Respaut & Lancelot, 1983). However, these ages are younger than the previously published ages of 314 ± 6 Ma (Respaut & Lancelot, 1983) and 307 ± 3 Ma (Guille et al., 2018). This may suggest that the Ansignan charnockite pluton was emplaced over a period of ~314–300 Ma, similar to the time period of emplacement of the Saint Arnac pluton.

Zircon rim U-Pb ages of ~290–310 Ma from the Riverole, Bélesta, and Caramany Gneisses suggest that the middle-lower crust underwent HT-LP metamorphism during the late Variscan orogeny and postorogenic extensional collapse (Deloule et al., 2002; Vissers, 1992; Vielzeuf, 1996). The zircon rims have significantly higher, often an order of magnitude, U/Th ratios (or low Th/U) than the cores and single age zircon grains, suggesting that the rims are metamorphic zircon growth. Additionally, a recent study by Guille and others shows that the rims in the gneisses are metamorphic based on cathodoluminescence images and trace element analysis (Guille et al., 2018). Based on zircon U-Pb data and petrological studies, there is no evidence for temperatures >700 °C after the Late Carboniferous (e.g., Olivier et al., 2008, and references within), which provides a maximum temperature constraint for basement units during the Early Cretaceous.

5.2. Post-Variscan: Permian-Early Cretaceous (Barremian)

The Agly Massif experienced cooling and minor exhumation in the Permian-Triassic associated with regional extension following the end of the Variscan orogeny (Chelalou et al., 2016; Puigdefabregas & Souquet, 1986; Vergés & García Senz, 2001). Thin and continuous carbonate platform deposition during the Late Triassic-Jurassic suggests a phase of tectonic quiescence characterized by stable, shallow marine conditions following Triassic rifting (Berger et al., 1993). The lithospheric attenuation was likely only minor during

Permian-Triassic extension as deduced from Triassic evaporite (Berger et al., 1993) and Jurassic to Early Cretaceous (Barremenian) carbonate deposition in near-isostatic equilibrium (Vacherat et al., 2016).

As for most of the Pyrenean realm during the early Mesozoic, the Agly Massif experienced slow subsidence and sediment accumulation, causing minor burial reheating during the Late Triassic-Early Cretaceous (~200–120 Ma), prior to renewed cooling and exhumation beginning in the late Aptian (e.g., Jammes et al., 2009; Lagabrielle et al., 2010; Vauchez, Clerc, et al., 2013; Vacherat et al., 2014).

5.3. Early Cretaceous Tectonic and Thermal Evolution

The apatite U-Pb data provide new geochronological constraints on the pre-Pyrenean exhumation history of the Agly Massif. The upper crust and middle-lower crustal rocks presently juxtaposed across a series of faults (including the Ansignan and Rentadou Faults; Figure 1) between the gneisses and pluton display drastically different prerift thermal histories from the Carboniferous to the Early Cretaceous. The data clearly illustrate that the structural juxtaposition of the units from very different crustal structural levels occurred during Aptian-Albian rifting in response to crustal thinning and hyperextension (Figure 7).

The data illustrate that the Saint Arnac pluton was emplaced into the upper crust and underwent rapid post-magmatic cooling in the Carboniferous and remained at temperatures well below 450 °C. In contrast, the middle-lower crust experienced high-T metamorphism during the Carboniferous and remained in the middle to lower crust at temperatures >450 °C until the Aptian. Apatite U-Pb ages from the Bélesta and Caramany Gneisses and the Ansignan Charnockite all exhibit Aptian cooling ages and flat single-grain age spectra (Figure 6), indicative of rapid cooling in response to extensional exhumation of the middle and lower crust. These exhumation ages agree well with reported timing estimates for the onset of rifting as constrained by basin subsidence and kinematic plate models for the western Pyrenees (e.g., Gong et al., 2008; Hart et al., 2017; Jammes et al., 2009; Masini et al., 2014).

The Riverole Gneiss have apatite U-Pb ages between those for the upper-crustal Saint Arnac pluton (~304–330 Ma) and the lower-crustal gneisses (~127–113 Ma) and are characterized by highly dispersed data and complex single grain U-Pb age spectra (Figure 6b). Single-grain age spectra show complex spatial apatite U-Pb age patterns that do not resemble square-pulse profiles, characteristic of rapid exhumation, or rounded diffusive profiles, suggestive of Pb diffusion during slow cooling. The scatter of ages consistently fall between a maximum of ~300 Ma and a minimum of ~110 Ma. Backscatter electron images show systematic brightness variations suggestive of overgrowth and internal domain recrystallization that appears to explain the bimodal age scattering evident in single-grain apatite age spectra. We interpret these complex age spectra with a lower bound corresponding to the age of exhumation of the lower crust (~110 Ma) and microtextures as related to apatite overgrowth and/or crack-and-seal-type deformation and recrystallization during shearing associated with crustal thinning during the Early Cretaceous.

It is important to stress that the abrupt change in apatite U-Pb ages across the present-day faults and Riverole Gneiss cannot represent an exhumed fossil apatite U-Pb partial retention zone based on the following observations: (1) the age gradient is too abrupt and narrow (<1 km), (2) single-grain age spectra do not exhibit well-behaved rounded concentration profiles suggestive of isothermal holding or slow cooling, and (3) the age spectra and microtextures exhibit clear intragrain bimodal age complexities likely caused by exhumation-related deformation.

Apatite U-Pb ages and associated square-profile age spectra from the high-grade Bélesta and Caramany Gneisses and the Ansignan Charnockite record rapid cooling and exhumation of middle-lower crustal rocks from >450 °C in the Aptian. The interpretation of rapid middle-lower crustal exhumation from >450 °C is supported by the following: (1) the Aptian-Albian cooling ages are only found in the structurally deepest parts of the massif and are in two separate N-S transects sharply delimited by the Riverole gneiss, (2) the apatite U-Pb ages predate Albian-Cenomanian monazite (98 ± 2 Ma) and titanite (110 ± 8 Ma) ages from albitites associated with hydrothermal fluid circulation (Poujol et al., 2010), mantle exhumation, and metamorphism/metasomatism in the Boucheville and Bas-Agly Basins, and (3) apatite U-Pb cooling ages from the upper-crustal St. Arnac pluton (304.4 ± 3.1 Ma) are not thermally reset, despite close proximity to the hydrothermally altered Lansac albitite with a monazite U-Pb age of 98 ± 2 Ma. These contrasting apatite cooling and hydrothermal monazite ages (Poujol et al., 2010) from the same area corroborate the fact that hydrothermal fluid circulation was spatially limited and localized

along discrete fluid pathways (Olivier, 2013). This resulted in Albian-Cenomanian recrystallization and growth and/or recrystallization of some accessory phases but not in wholesale post-Aptian reheating the Agly massif. This conclusion is also supported by new rutile U-Pb data presented here from the Bélesta Gneiss (~103–107 Ma). While rutile trace element data indicate a felsic source and metamorphic temperatures of ~650 °C of the protolith, the rutile U-Pb age is younger than the corresponding apatite U-Pb ages and consistent with subclosure temperature recrystallization during localized hydrothermal circulation. Ayers and Watson (1991) showed that rutile is much more soluble than apatite in the presence of supercritical aqueous fluids, as fluids can dissolve significant amounts of Ti but very little phosphate (Ayers & Watson, 1991). This supports our interpretation that the rutile U-Pb ages in the Bélesta Gneiss record recrystallization likely associated with localized fluid circulation and explains the younger rutile U-Pb ages than apatite U-Pb ages in the Bélesta Gneiss.

We propose a three-stage thermomechanical evolution for the Agly Massif during progressive rifting and crustal breakup motivated by the current understanding of fossil rift margins and numerical models and the integration of the new thermochronological data and existing structural evidence from the Agly Massif (Figure 8).

5.3.1. Decoupled Thinning and Necking Phase: Late Aptian (122.5–113 Ma)

The onset of major upper-crustal extension appears to postdate earliest Aptian shallow-marine platform carbonate sedimentation. During the middle Aptian (~122.5 Ma), sedimentary facies in the region began to change with the deposition of Gargasian limestone to calcareous marl, signaling rapid basin subsidence (Berger et al., 1993). This accelerated synrift subsidence marks the onset of major upper-crustal extension, which is attributed to either progressive thinning or likely the onset crustal necking.

Apatite U-Pb cooling ages for the high-grade gneisses indicate major exhumation as the middle crust was rapidly thinned out along a crustal-scale shear zone in the middle crust (Figure 8a). This is also supported by 100- to 130-Ma biotite Rb-Sr ages (T_c = 300–380 °C) from the gneisses (Roubault et al., 1963). The new thermochronometric data document a major structural and thermal discontinuity between the high-grade gneisses that resided in the middle-lower crust until the Early Cretaceous and the upper crustal Saint Arnac pluton. This relationship could be explained by a continentward, north dipping shear zone juxtaposing the two structural levels. Olivier et al. (2008) documented an extensional mylonitic shear zone at the base of the Saint Arnac pluton that they related to thinning and or/extension during the Carboniferous. Vauchez, Clerc, et al. (2013) document north to northeast dipping extensional shear zones with mylonites that show with evidence of deformation at the ductile-brittle transition. Given the new thermochronometric data, it is likely that these mylonites at least in part are related to crustal thinning during the Early Cretaceous that eventually juxtaposed the gneisses and Saint Arnac pluton. The Riverole Gneiss appears to represent an upper-middle crustal sliver within or adjacent to the shear zone based on the apatite U-Pb data. Exhumation of the gneisses is accommodated by shear localization in the middle crust (Mohn et al., 2012) within the necking domain and likely some amount of lower crustal boudinage (Clerc et al., 2014; Figure 8a). Upper- and lower-crustal deformation remained decoupled along a midcrustal shear zone as evidenced by the different thermal histories recoded in upper crustal Saint Arnac Pluton and middle-lower crustal gneisses (Figure 8). The decoupled thinning phase lead to ductile attenuation of the middle-lower crust. This thinning resulted in compression of metamorphic isograds in the gneisses and preservation of the high present-day apparent temperature gradient of ~100 °C/km (Delay, 1990; Olivier et al., 2004; Guille et al., 2018).

5.3.2. Coupled Thinning and Extraction Phase: Earliest Albian (113–110 Ma)

Progressive extension and crustal attenuation eventually lead to mechanical coupling and juxtaposition of upper and lower crustal units by semiductile to brittle shearing and faulting (Figure 8b; e.g., Lavier & Manatschal, 2006; Manatschal et al., 2015; Sutra & Manatschal, 2012). This was accommodated by a continentward dipping extensional shear zone that acted as extraction faults, rapidly exhuming the lower crust and bringing these granulitic gneisses to upper-crustal structural level by early Albian times. The final juxtaposition of the high-temperature gneisses and upper-crustal granites must have occurred by brittle deformation as there is no evidence for contact reheating of the upper-crustal unit across the units. This implies that structural abutment of the middle and lower crust occurred when both units had already cooled well below 450 °C, based on the apatite U-Pb data. This brittle extraction fault is in a position now occupied by the Rentadou Fault, which was likely reactivated during the Pyrenean orogeny (Figure 1). Similar continent-dipping shear zones have been observed in other hyperextended margins but have variably

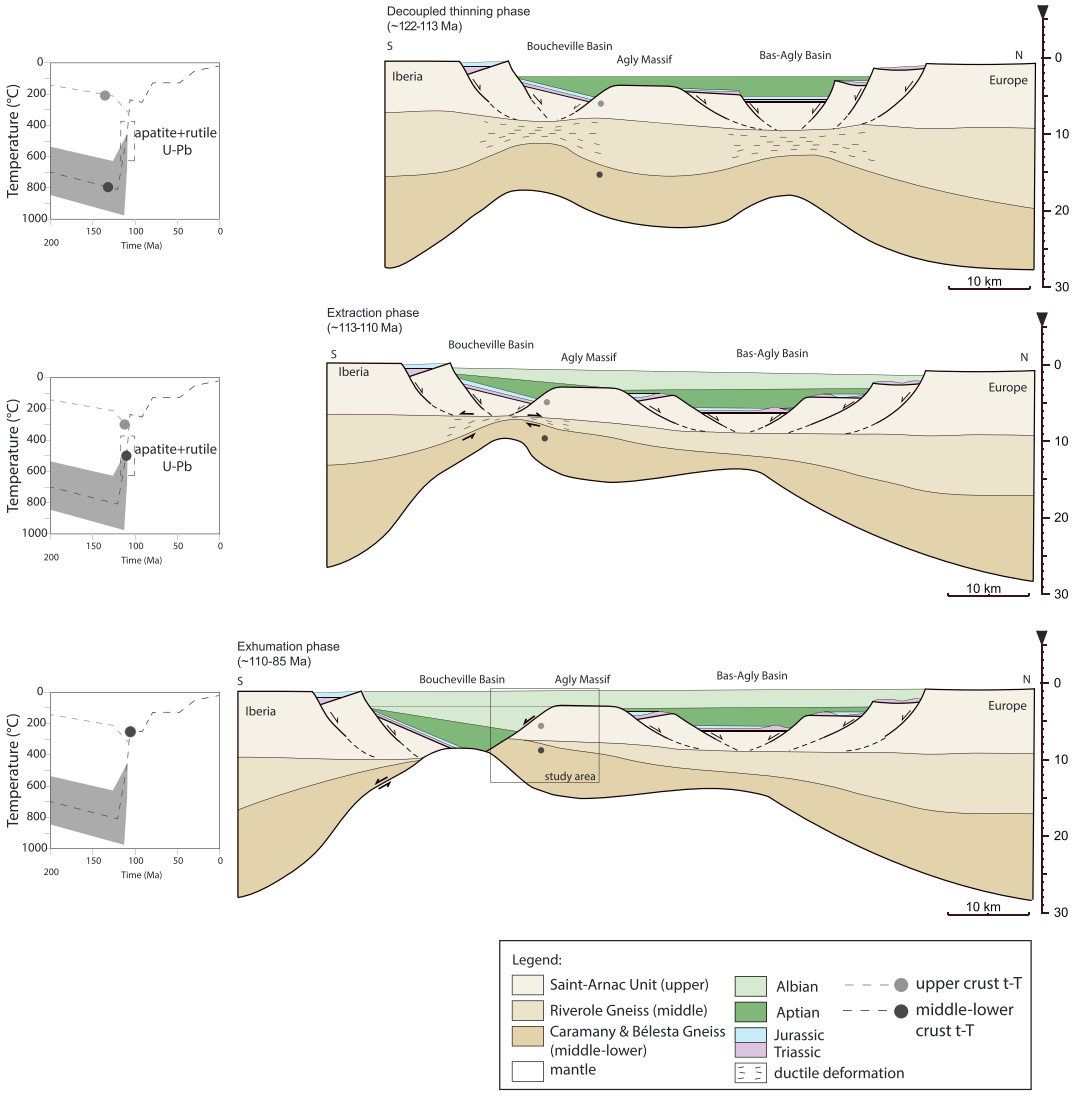

Figure 8. Schematic cross sections of the Iberia-European margin in the Aptian-Cenomanian showing key the interpreted structural evolution of the continental crust during progressive rifting and hyperextension.

been interpreted either as older orogenic shear zones or as synextensional extraction faults due to lack of clear timing relationships (e.g., the Louhossoa lineament in the Western Pyrenees; Jammes et al., 2009; Masini et al., 2014). In the Agly massif, the U-Pb apatite data unequivocally demonstrate an Early Cretaceous synrift nature for this structural juxtaposition.

5.3.3. Exhumation Phase: Albian-Cenomanian (110–85 Ma)

In rifting models, mechanical coupling of the crust in the brittle realm results in a fundamental change in mechanical behavior, culminating in the formation of a major detachment fault systems (e.g., Lavier & Manatschal, 2006). The formation of concave-up, lithospheric-scale "exhumation faults" marks the onset of crustal separation, eventual mantle exhumation, and possible oceanic breakup (e.g., Lavier & Manatschal, 2006; Manatschal, 2004; Masini et al., 2014; Péron-Pinvidic et al., 2007; Reston & McDermott, 2011; Tugend et al., 2014). The mechanical coupling of the two structural units (upper crust pluton and middle-lower crust high-grade gneisses) is supported by the shared thermal histories of the two units beginning in the Albian recorded by zircon and apatite (U-Th)/He analysis and thermal modeling (Ternois et al., 2019).

The boundary between the Boucheville Basin and the high-grade gneisses is marked by a major subvertical fault that appears to have acted as a reverse fault during Pyrenean deformation but has been interpreted by

several previous studies as a major synrift, south dipping extensional or detachment fault (Chelalou et al., 2016; Vauchez, Clerc, et al., 2013). This interpretation is supported by (1) the significant structural throw across this fault that juxtaposes Aptian-Albian sediments to the south against the exhumed middle-lower crustal Caramany Gneiss and Ansignan charnockite units to the north necessitating significant normal motion along the fault in the Cretaceous, (2) elevated thermal regime in the Boucheville Basin attributed to high-temperature metamorphism during mantle exhumation (Vauchez, Clerc, et al., 2013; Clerc & Lagabrielle, 2014; Clerc, Lahfid, et al., 2015; Chelalou et al., 2016), and (3) the along-strike exposure of exhumed subcontinental mantle in the Salvezines massif (Clerc et al., 2014, and references within).

Given these lines of evidence, we interpret this fault as a detachment fault that cut across the upper crustal Agly block, truncated the earlier semibrittle extraction fault zone, and eventually exhumed subcontinental mantle (Figure 8c). This structural geometry and evolution are largely based on models of rifting (e.g., Lavier & Manatschal, 2006; Péron-Pinvidic & Manatschal, 2010; Whitmarsh et al., 2001), but this proposed evolution is supported by timing of mantle exhumation and emplacement in the Agly region in the late Albian (Golberg et al., 1986; Henry et al., 1998). Importantly, the apatite U-Pb data do not record this unroofing and show that exhumation along detachment faults was of limited magnitude as the lower-plate Agly gneisses were already exhumed to an upper-crustal position in Aptian times. Subcontinental mantle is thought to have been exhumed and emplaced.

Final rift-related exhumation of the Agly crustal block was likely enhanced by a minor north dipping detachment between the Agly massif and the overlying sedimentary strata of the Bas-Agly Basin to the north evident by microstrucutres typical of ductile deformation in the overlying Triassic-Jurassic rocks (Vauchez, Clerc, et al., 2013). The thermochronometric data allow for only limited upper-crustal tectonic unroofing along the northern massif margin as no thermochronometers in the footwall record this exhumation. During the mantle exhumation phase in the late Albian and early Cenomanian, the Boucheville Basin rapidly deepened and accommodated widespread deposition of the marl and black turbidites of the "flysch noir" (Berger et al., 1993; Chelalou et al., 2016).

5.4. Basement and Basin Thermal History Disconnect

Mantle exhumation appears to have been accompanied by HT-LP metamorphism of prerift and synrift sedimentary strata in extensional basins associated with exhumed mantle domains, localized basement metasomatism, and late synrift alkaline magmatism dated between 110 and 90 Ma (e.g., Boutin et al., 2016; Clerc et al., 2016; Golberg et al., 1986; Hart et al., 2017; Montigny et al., 1986; Vacherat et al., 2016). The HT-LP metamorphism of Mesozoic prerift and synrift strata occurred at 110–85 Ma, with the peak of HT-LP metamorphism at ~95 Ma, with maximum temperatures of up to 550–650 °C (Albarède & Michard-Vitrac, 1978; Bernus Maury, 1984; Boulvais, 2016; Clerc & Lagabrielle, 2014; Chelalou et al., 2016; Clerc, Lahfid, et al., 2015, 2016; Corre et al., 2016; Golberg et al., 1986; Golberg & Leyreloup, 1990; Montigny et al., 1986; Vauchez, Clerc, et al., 2013).

In the Agly domain, prerift and synrift strata experienced peak temperatures at ~100–95 Ma of 450–600 °C in the Boucheville Basin, significantly lower temperatures of 300–400 °C in the Bas-Agly Basin, and negligible heating in the St. Paul Fenouillet Syncline to the NW of the Agly Massif (Clerc, Lahfid, et al., 2015; Chelalou et al., 2016; Olivier, 2015; Vauchez, Clerc, et al., 2013; Vauchez, Chauvet, et al., 2013). Synrift basinal reheating is thought to have occurred above narrow exhumed mantle domains with heating focused between crustal blocks (Lagabrielle et al., 2010). In addition to HT-LP metamorphism, the heating resulted in the advection of the brittle-ductile transition in the Boucheville and Bas-Agly Basins as evidenced by the ductile deformation of deeply buried portions of the basins (Clerc et al., 2016; Légier et al., 1987; Vauchez, Clerc, et al., 2013; Vauchez, Chauvet, et al., 2013). This represents the final phase of deformation associated with rifting in the distal domain (Pérez-Gussinyé & Reston, 2001).

The discrepancy between basement and basin temperature estimates and thermal histories attributed to the difference in exhumational conductive cooling and younger hydrothermal fluid circulation is not unique to the Agly Massif. In the Saint Barthelemy Massif of north central Pyrenees, a similar difference in the thermal histories of the basement and basins is observed, where medium- to low-temperature (250–350 °C) metasomatism altered the basement, while high-temperature (500–600 °C) metamorphism affected the Mesozoic cover during the Albian-Cenomanian (Boutin et al., 2016). This implies that either (1) continental crustal separation or mantle exhumation in the basinal domain occurred prior to Albian-Cenomanian HT-LP

metamorphism (e.g., Clerc & Lagabrielle, 2014; Clerc & Lagabrielle, 2015), (2) that the metamorphism was due to circulation of hot fluids through permeable sedimentary rocks in the basins and had less of an effect on low-permeability basement rocks, (3) peak temperatures recorded by Raman spectroscopy of carbonaceous material (RSCM; Chelalou et al., 2016, and references within) were only transient and insufficient in duration to reset apatite U-Pb or zircon (U-Th)/He thermochronometers, or (4) the Boucheville Basin was telescoped during Pyrenean shortening, juxtaposing the distal margin where temperatures were higher to its present location in contact with the more proximal margin of Agly basement. The possibility that the Boucheville Basin was structurally telescoped, however, would not explain high metamorphism in the Bas-Agly syncline, to the north of the massif, nor discrete hydrothermal alteration in the Agly basement. The lack of thermochronometric constraints, specifically apatite U-Pb and zircon (U-Th)/He, on the thermal history of the Boucheville and Bas-Agly Basins hampers determination between these different scenarios.

5.5. Implications for Rifting Models

The findings of this study constrain the structural and thermal evolution of the middle and lower crust in the Agly Massif during hyperextension, which is critical to assessing the importance and timing of key structures. After initial thinning of the middle to lower crust, accompanied by diffuse upper-crustal extension during the stretching phase, the crust was thinned to ~10 km along a midcrustal shear zone during necking and the decoupled extensional phase. This was accommodated by brittle extension of the upper crust and ductile thinning of the lower crust, overall resulting in the advection and exhumation of the middle-lower crust. The onset of rapid basin subsidence likely signals the inception of lithospheric necking during decoupled hyperextension.

In the necking zone of the Agly crustal block, this exhumation appears to have been principally accommodated by a continent-dipping fault zone, acting as an extraction fault, and progressively leading to mechanical coupling. These structures are analogous to CDNF have been imaged in seismic profiles across modern rifted continental margins and been attributed to the ductile to semibrittle juxtaposition of upper and lower crust. Motion along this extraction fault in the Agly Massif, separating the lower-crustal gneisses and the upper-crustal granites, appears to be responsible for the majority of exhumation of the middle-lower crust and bringing the middle-lower crustal rocks in the distal continental margin into an upper-crustal position. This is important as it is often unclear whether lower-crustal rocks in distal margins were exhumed during previous orogenic events or during hyperextension. The new data unequivocally demonstrate that the high-grade gneisses were not exhumed and juxtaposed against the upper-crustal rocks during the Variscan orogeny but during Cretaceous coupled hyperextension.

Mechanically coupled hyperextension led to a fundamental change in the mechanical and rheological behavior of the crust/lithosphere, culminating in the formation of major, oceanward dipping low-angle detachment fault that accommodates crustal separation, exhumation of the mantle, and hydrothermal reheating of the supradetachment basins in the distal margin and mantle exhumation domain. Based on the temporal constraints of middle-lower crustal exhumation, the structural relationship between the basement and Boucheville Basin, and Boucheville Basin depositional records, the detachment faulting postdates the juxtaposition of lower and upper crust and must crosscut the extraction fault zone. This is corroborated by the fact that mantle exhumation and accompanying hydrothermal heating of both basin and distal continental margin postdate middle-lower crustal exhumation by >10–15 Myr. The timing sequence of hyperextensional coupling followed by mantle exhumation and break-up appears to be supported by numerical models (e.g., Lavier & Manatschal, 2006; Brune et al. 2014), Hence, the results from the Agly Massif provide important and transportable insights into the temporal, thermal, and geometric evolution of rifted margins during the transitions from coupled to decoupled hyperextension and to crustal separation and mantle exhumation.

Furthermore, the eastern NPZ has been proposed as an example of a “hot paleomargin” with ductile crustal boundinage (Clerc et al., 2014; Clerc, Lahfid, et al., 2015; Vauchez, Clerc, et al., 2013). Apatite U-Pb data along with zircon (U-Th)/He data (Odlum & Stockli, 2017; Ternois et al., 2019) demonstrate that the lower- and upper-crustal basement gneisses and granites had rapidly cooled to <<450 °C by the early Albian and were subsequently never reheated to >300 °C. The exposed gneisses and granites had cooled below the brittle-ductile transition by the early Albian and could not have undergone ductile crustal-scale boudinage after the early Albian. However, Vauchez, Clerc, et al. (2013) showed that the sedimentary cover underwent ductile deformation during the Albian-Cenomanian during the interpreted heating of the basins (Chelalou et al.,

2016). This disparity suggests very different thermal regimes and rheological behavior of continental basement rocks of the distal margin and sedimentary basins associated with the distal margin and exhumed mantle domains. This implication is also supported by findings from the Saint Barthelemy Massif to the west, where there is evidence that suggests a structural decoupling between the basement and the Mesozoic cover, and the breakoff of the crust and mantle along a major detachment fault (Boutin et al., 2016).

In the Agly Massif, the CDNF shear zone, or high temperature top-to-the-continent shear zone (Manatschal, 2004) accommodated extension associated with a crustal-scale shear affecting the entire crust leading to extreme thinning and lateral juxtaposition of lower and upper crust. Once brought to shallow levels in the brittle field, the middle to lower crust was mechanically coupled with the upper crust and exhumation was controlled by a "cold" top to the ocean fault (e.g., Clerc, Jolivet, & Ringenbach, 2015; Jolivet et al., 2015; Manatschal, 2004). The medium to high temperature thermochronology data demonstrate that the Agly Massif is an excellent example of proposed models invoking a three-layer continental crust with strong upper and lower crust strongly decoupled by a weaker, ductile middle crust for the evolution of magma poor rifted margins (Lavier & Manatschal, 2006; Manatschal, 2004; Mohn et al., 2012; Péron-Pinvidic et al., 2007; Péron-Pinvidic & Manatschal, 2009) and illustrates the power of apatite U-Pb thermochronology to understand middle to lower crustal processes and provide constraints in systems where low-temperature thermochronometers are overprinted by younger tectonic events.

6. Conclusions

Zircon, apatite, and rutile U-Pb geoochronometric and thermochronometric data provide new first-order constraints on the structural and thermal evolution of Early Cretaceous hyperextension in the Eastern Pyrenean domain. The data ascertain that extreme crustal thinning and mylontization occurred in the Early Cretaceous during hyperextension. Zircon U-Pb ages across the massif record the complex magmatic and metamorphic history of the continental crust. The apatite and rutile U-Pb ages record the onset of exhumation of the middle and lower crust beginning in the early Aptian, during which upper- and lower-crustal extension was decoupled along a midcrustal, continent-dipping shear zone, and the crust was significantly thinned. Following the Aptian thinning phase, the massif was then exhumed along a south dipping fault at the southern boundary of the massif (fault controlling the opening of the Boucheville Basin) and enhanced by a second north dipping detachment at the northern boundary of the massif. Exhumation of the mantle and associated HT-LP metamorphism of the prerift and synrift sedimentary strata and metasomatism of the basement occurred during the Albian and continued through the Cenomanian. The data show the juxtaposition of the upper crustal pluton with the middle-lower crustal gneisses occurred in the Aptian-Albian and that the basement did not experience reheating associated with mantle exhumation and remained <<450 °C coeval with the HT metamorphism of the prerift and synrift sedimentary strata. The apatite U-Pb ages overlap with some zircon (U-Th)/He ages (Odlum & Stockli, 2017; Ternois et al., 2019) suggesting that the middle-lower crust was exhumed to ~200–180 °C (T_c of zircon (U-Th)/He)), where the basement remained from Albian time to the onset of shortening in the Santonian. The new data presented here, along with published data, demonstrate that crustal thinning occurred in the Early Cretaceous and provide a timeline of processes associated with hyperextension and mantle exhumation in the distal margin and provides an analog for the evolution of modern-day passive margins.

Acknowledgments
The authors would like to thank Lisa Stockli, Tomas Capaldi, Doug Barber, Federico Galster, Rudra Chatterjee, Kelly Thomson, and Patrick Boyd for assistance in data acquisition, reduction, and interpretation. We extend gratitude to Sébastien Ternois, Mary Ford, Raphaël Pik, Frederic Mouthereau, and other members of the OROGEN project for helpful scientific discussions. The manuscript greatly benefited from reviews from Claudio Rosenberg and an anonymous reviewer. This research was funded by the Geological Society of America, American Association of Petroleum Geologists, Jackson School of Geosciences at the University of Texas at Austin (grants awarded to M. L. O.), an Equinor Fellowship (M. L. O.), and by UTChron at the University of Texas (P. I. Daniel Stockli). Sample locations, data tables, and extended methodology can be found in the supporting information.

References

Aguilar, C., Liesa, M., Castiñeiras, P., & Navidad, M. (2014). Late Variscan metamorphic and magmatic evolution in the eastern Pyrenees revealed by U–Pb age zircon dating. *Journal of the Geological Society*, *171*(2), 181–192. https://doi.org/10.1144/jgs2012-086

Albarède, F., & Michard-Vitrac, A. (1978). Age and significance of the North Pyrenean metamorphism. *Earth and Planetary Science Letters*, *40*(3), 327–332. https://doi.org/10.1016/0012-821X(78)90157-7

Albarède, F., & Michard-Vitrac, A. (1978). Datation du metamorphisme des terrains secondaires des Pyrenees par les methodes 39 Ar-40 Ar et 87 Rb-87 Sr; ses relations avec les peridotites associees. *Bulletin de la Société Géologique de France*, *7*(5), 681–687.

Andrieux, P. (1982a). Conditions de cristallisation et évolution paragénétique d'une charnockite hercynienne: Le complexe granulitique d'Ansignan (massif de l'Agly, Pyrénées-Orientales). *Bulletin de Mineralogie*, *105*, 253–266.

Andrieux, P. (1982b). La Charnockite d'Ansignan: Massif de l'Agly-Pyrénées orientales: mise en place et évolution paragénétique, introduction à l'étude des équilibres grenat-orthopyroxène (Doctoral dissertation, Impr. UER Sci.).

Avigad, D., Gerdes, A., Morag, N., & Bechstädt, T. (2012). Coupled U–Pb–Hf of detrital zircons of Cambrian sandstones from Morocco and Sardinia: Implications for provenance and Precambrian crustal evolution of North Africa. *Gondwana Research*, *21*(2–3), 690–703. https://doi.org/10.1016/j.gr.2011.06.005

Ayers, J. C., & Watson, E. B. (1991). Solubility of apatite, monazite, zircon, and rutile in supercritical aqueous fluids with implications for subduction zone geochemistry. *Philosophical Transactions of the Royal Society of London A*, *335*(1638), 365–375.
Barbosa, J., & Fonteilles, M. (1986). Examen critique des résultats fournis par certains baromètres couramment utilisés en terrains granulitiques: exemples des granulites de Bahia (Brésil) et du massif de L'Agly (France). *Bulletin de Mineralogie*, *109*(4), 359–376. https://doi.org/10.3406/bulmi.1986.7946
Barnolas, A., Chiron, J. C., & Guérangé, B. (Eds.) (1996). *Synthèse géologique et géophysique des Pyrénées: géophysique: cycle hercynien*. Orléans, France: BRGM.
Beltrando, M., Stockli, D. F., Decarlis, A., & Manatschal, G. (2015). A crustal-scale view at rift localization along the fossil Adriatic margin of the Alpine Tethys preserved in NW Italy. *Tectonics*, *34*, 1927–1951. https://doi.org/10.1002/2015TC003973
Berger, G. M., Fonteilles, M., Leblanc, D., Clauzon, G., Marchal, J. P., & Vautrelle, C. (1993). Notice explicative de la feuille Rivesaltes à 1/50 000.
Bernus Maury, C. (1984). Etude des paragéneses caractéristiques du métamorphisme mésozoïque dans la partie orientale des Pyrénées (Doctoral dissertation).
Bouhallier, H., Choukroune, P., & Ballèvre, M. (1991). Évolution structurale de la croûte profonde Hercynienne: Exemple du massif de l'Agly (Pyrénées Orientales, France). *Comptes Rendus de l'Académie des Sciences*, *312*, 647–654.
Boulvais, P. (2016). Fluid generation in the Boucheville Basin as a consequence of the North Pyrenean metamorphism. *Comptes Rendus Géoscience*, *348*(3–4), 301–311. https://doi.org/10.1016/j.crte.2015.06.013
Boulvais, P., De Parseval, P., D'Hulst, A., & Paris, P. (2006). Carbonate alteration associated with talc-chlorite mineralization in the eastern Pyrenees, with emphasis on the St. Barthelemy Massif. *Mineralogy and Petrology*, *88*(3–4), 499–526. https://doi.org/10.1007/s00710-006-0124-x
Boulvais, P., Ruffet, G., Cornichet, J., & Mermet, M. (2007). Cretaceous albitization and dequartzification of Hercynian peraluminous granite in the Salvezines Massif (French Pyrénées). *Lithos*, *93*(1–2), 89–106. https://doi.org/10.1016/j.lithos.2006.05.001
Boutin, A., de Saint Blanquat, M., Poujol, M., Boulvais, P., De Parseval, P., Rouleau, C., & Robert, J. F. (2016). Succession of Permian and Mesozoic metasomatic events in the eastern Pyrenees with emphasis on the Trimouns talc–chlorite deposit. *International Journal of Earth Sciences*, *105*(3), 747–770. https://doi.org/10.1007/s00531-015-1223-x
Boyd, P. D., Galster, F., & Stockli, D. F. (2017). Intra-grain common Pb correction and detrital apatite U-Pb dating via LA-ICPMS depth profiling. In AGU Fall Meeting Abstracts, December 2017.
Brun, J. P., & Beslier, M. O. (1996). Mantle exhumation at passive margins. *Earth and Planetary Science Letters*, *142*(1–2), 161–173. https://doi.org/10.1016/0012-821X(96)00080-5
Brune, S., Heine, C., Pérez-Gussinyé, M., & Sobolev, S. V. (2014). Rift migration explains continental margin asymmetry and crustal hyperextension. *Nature Communications*, *5*(1), 4014. https://doi.org/10.1038/ncomms5014
Casas, J. M., Castiñeiras, P., Navidad, M., Liesa, M., & Carreras, J. (2010). New insights into the Late Ordovician magmatism in the Eastern Pyrenees: U–Pb SHRIMP zircon data from the Canigó massif. *Gondwana Research*, *17*(2–3), 317–324. https://doi.org/10.1016/j.gr.2009.10.006
Casas, J. M., & Murphy, J. B. (2018). Unfolding the arc: The use of pre-orogenic constraints to assess the evolution of the Variscan belt in Western Europe. *Tectonophysics*, *736*, 47–61.
Chamberlain, K. R., & Bowring, S. A. (2001). Apatite–feldspar U–Pb thermochronometer: A reliable, mid-range (~ 450° C), diffusion-controlled system. *Chemical Geology*, *172*(1–2), 173–200. https://doi.org/10.1016/S0009-2541(00)00242-4
Chelalou, R., Nalpas, T., Bousquet, R., Prevost, M., Lahfid, A., Poujol, M., et al. (2016). New sedimentological, structural and paleothermicity data in the Boucheville Basin (eastern North Pyrenean Zone, France). *Comptes Rendus Géoscience*, *348*(3–4), 312–321. https://doi.org/10.1016/j.crte.2015.11.008
Cherniak, D. J. (2000). Pb diffusion in rutile. *Contributions to Mineralogy and Petrology*, *139*(2), 198–207. https://doi.org/10.1007/PL00007671
Chew, D. M., Petrus, J. A., & Kamber, B. S. (2014). U–Pb LA–ICPMS dating using accessory mineral standards with variable common Pb. *Chemical Geology*, *363*, 185–199. https://doi.org/10.1016/j.chemgeo.2013.11.006
Choukroune, P. (1974). Structure and tectonic evolution of the North-Pyrenean zone: analysis of the deformation in a portionof chain with sub-vertical schistosity (Doctoral dissertation, University of Sciences and Techniques ofLanguedoc).
Clerc, C., Jolivet, L., & Ringenbach, J. C. (2015). Ductile extensional shear zones in the lower crust of a passive margin. *Earth and Planetary Science Letters*, *431*, 1–7. https://doi.org/10.1016/j.epsl.2015.08.038
Clerc, C., & Lagabrielle, Y. (2014). Thermal control on the modes of crustal thinning leading to mantle exhumation: Insights from the Cretaceous Pyrenean hot paleomargins. *Tectonics*, *33*, 1340–1359. https://doi.org/10.1002/2013TC003471
Clerc, C., Lagabrielle, Y., Labaume, P., Ringenbach, J. C., Vauchez, A., Nalpas, T., et al. (2016). Basement-cover decoupling and progressive exhumation of metamorphic sediments at hot rifted margin. *Tectonophysics*, *686*, 82–97. https://doi.org/10.1016/j.tecto.2016.07.022
Clerc, C., Lagabrielle, Y., Lahfid, A., Vauchez, A., Labaume, P., & Bousquet, R. (2014). Extreme thinning of the continental crust and mantle exhumation at passive margins. Constraints from the Pyrenean analog. In *24 ème Réunion des sciences de la Terre 2014* (p. 227).
Clerc, C., Lahfid, A., Monié, P., Lagabrielle, Y., Chopin, C., Poujol, M., et al. (2015). High-temperature metamorphism during extreme thinning of the continental crust: A reappraisal of the North Pyrenean paleo-passive margin. *Solid Earth Discussions*, *6*(2), 643–668. https://doi.org/10.5194/se-6-643-2015
Clerc, C., Ringenbach, J. C., Jolivet, L., & Ballard, J. F. (2018). Rifted margins: Ductile deformation, boudinage, continentward-dipping normal faults and the role of the weak lower crust. *Gondwana Research*, *53*, 20–40. https://doi.org/10.1016/j.gr.2017.04.030
Corre, B., Lagabrielle, Y., Labaume, P., Fourcade, S., Clerc, C., & Ballèvre, M. (2016). Deformation associated with mantle exhumation in a distal, hot passive margin environment: New constraints from the Saraillé Massif (Chaînons Béarnais, North-Pyrenean Zone). *Comptes Rendus Géoscience*, *348*(3–4), 279–289. https://doi.org/10.1016/j.crte.2015.11.007
Dahl, P. S. (1997). A crystal-chemical basis for Pb retention and fission-track annealing systematics in U-bearing minerals, with implications for geochronology. *Earth and Planetary Science Letters*, *150*(3–4), 277–290. https://doi.org/10.1016/S0012-821X(97)00108-8
Dauteuil, O., & Ricou, L. E. (1989). Une circulation de fluides de haute-température à l'origine du métamorphisme crétacé nord-pyrénéen. *Geodinamica Acta*, *3*(3), 237–249. https://doi.org/10.1080/09853111.1989.11105190
Davis, M., & Kusznir, N. J. (2004). Depth-dependent lithospheric stretching at rifted continental margins. In *Proceedings of NSF Rifted Margins Theoretical Institute*, (Vol. 136, p. 92). New York: Columbia University Press.
De Saint Blanquat, M., Lardeaux, J. M., & Brunel, M. (1990). Petrological arguments for high-temperature extensional deformation in the Pyrenean Variscan crust (Saint Barthélémy Massif, Ariège, France). *Tectonophysics*, *177*(1–3), 245–262. https://doi.org/10.1016/0040-1951(90)90284-F

Delay, F. (1990). Etude structurale du massif de l'Agly (Pyrénées orientales). Mémoires de la Société Géologique du Nord, 17.
Delay, F., & Paquet, J. (1989). Tectonique ductile en extension dans le massif hercynien de l'Agly (zone nord-pyrénéenne): Comptes Rendus de l'Académie des Sciences) (Vol. 308, pp. 1637–1643).
Deloule, E., Alexandrov, P., Cheilletz, A., Laumonier, B., & Barbey, P. (2002). In-situ U–Pb zircon ages for Early Ordovician magmatism in the eastern Pyrenees, France: The Canigou orthogneisses. *International Journal of Earth Sciences*, *91*(3), 398–405. https://doi.org/10.1007/s00531-001-0232-0
Denèle, Y., Laumonier, B., Paquette, J. L., Olivier, P., Gleizes, G., & Barbey, P. (2014). Timing of granite emplacement, crustal flow and gneiss dome formation in the Variscan segment of the Pyrenees. *Geological Society, London, Special Publications*, *405*. SP405-5
Driscoll, N. W., & Karner, G. D. (1998). Lower crustal extension across the Northern Carnarvon basin, Australia: Evidence for an eastward dipping detachment. *Journal of Geophysical Research*, *103*(B3), 4975–4991. https://doi.org/10.1029/97JB03295
Fabriès, J., Lorand, J. P., Bodinier, J. L., & Dupuy, C. (1991). Evolution of the upper mantle beneath the Pyrenees: Evidence from orogenic spinel lherzolite massifs. *Journal of Petrology*, *2*, 55–76.
Fallourd, S., Poujol, M., Boulvais, P., Paquette, J. L., de Saint Blanquat, M., & Rémy, P. (2014). In situ LA-ICP-MS U–Pb titanite dating of Na–Ca metasomatism in orogenic belts: The North Pyrenean example. *International Journal of Earth Sciences*, *103*(3), 667–682. https://doi.org/10.1007/s00531-013-0978-1
Fonteilles, M. (1976). Essai d'interprétation des compositions chimiques des roches d'origines métamorphique et magmatique du Massif hercynien de l'Agly (Pyrénées orientales). *I. II* (Doctoral dissertation).
Fonteilles, M., Leblanc, D., Clauzon, G., Vaudin, J.-L., & Berger, G.-M. (1993). Carte géologique de la France au 1/50.000, feuille de Rivesaltes (1090), Orléans: BRGM.
Golberg, J. M., & Leyreloup, A. F. (1990). High temperature-low pressure Cretaceous metamorphism related to crustal thinning (Eastern North Pyrenean Zone, France). *Contributions to Mineralogy and Petrology*, *104*(2), 194–207. https://doi.org/10.1007/BF00306443
Golberg, J. M., & Maluski, H. (1988). Données nouvelles et mise au point sur l'âge du métamorphisme pyrénéen. Comptes rendus de l'Académie des sciences. *Série 2, Mécanique, Physique, Chimie, Sciences de l'univers, Sciences de la Terre*, *306*(6), 429–435.
Golberg, J. M., Maluski, H., & Leyreloup, A. F. (1986). Petrological and age relationship between emplacement of magmatic breccia, alkaline magmatism, and static metamorphism in the North Pyrenean Zone. *Tectonophysics*, *129*(1–4), 275–290. https://doi.org/10.1016/0040-1951(86)90256-8
Gong, Z., Langereis, C. G., & Mullender, T. A. T. (2008). The rotation of Iberia during the Aptian and the opening of the Bay of Biscay. *Earth and Planetary Science Letters*, *273*(1–2), 80–93. https://doi.org/10.1016/j.epsl.2008.06.016
Grool, A. R., Ford, M., Vergés, J., Huismans, R. S., Christophoul, Y., & Dielforder, A. (2018). Insights Into the Crustal-Scale Dynamics of a Doubly Vergent Orogen From a Quantitative Analysis of Its Forelands: A Case Study of the Eastern Pyrenees. *Tectonics*, *37*(2), 450–476. https://doi.org/10.1002/2017TC004731
Guille, B. T., Olivier, P., Paquette, J. L., Bosse, V., & Guillaume, D. (2018). Evolution of the middle crust of the Pyrenees during the Paleozoic: new data on the plutonic rocks from the North Pyrenean Agly Massif. *International Journal of Earth Sciences*, *108*(1), 245–265.
Hart, N. R., Stockli, D. F., & Hayman, N. W. (2016). Provenance evolution during progressive rifting and hyperextension using bedrock and detrital zircon U-Pb geochronology, Mauléon Basin, western Pyrenees. *Geosphere*, *12*(4), 1166–1186. https://doi.org/10.1130/GES01273.1
Hart, N. R., Stockli, D. F., Lavier, L. L., & Hayman, N. W. (2017). Thermal evolution of a hyperextended rift basin, Mauléon Basin, western Pyrenees. *Tectonics*, *36*, 1103–1128. https://doi.org/10.1002/2016TC004365
Henry, P., Azambre, B., Montigny, R., Rossy, M., & Stevenson, R. K. (1998). Late mantle evolution of the Pyrenean sub-continental lithospheric mantle in the light of new 40Ar–39Ar and Sm–Nd ages on pyroxenites and peridotites (Pyrenees, France). *Tectonophysics*, *296*(1–2), 103–123. https://doi.org/10.1016/S0040-1951(98)00139-5
Huismans, R., & Beaumont, C. (2011). Depth-dependent extension, two-stage breakup and cratonic underplating at rifted margins. *Nature*, *473*(7345), 74–78. https://doi.org/10.1038/nature09988
Huismans, R. S., & Beaumont, C. (2008). Complex rifted continental margins explained by dynamical models of depth-dependent lithospheric extension. *Geology*, *36*(2), 163–166. https://doi.org/10.1130/G24231A.1
Huismans, R. S., & Beaumont, C. (2014). Rifted continental margins: The case for depth-dependent extension. *Earth and Planetary Science Letters*, *407*, 148–162.
Jackson, S. E., Pearson, N. J., Griffin, W. L., & Belousova, E. A. (2004). The application of laser ablation-inductively coupled plasma-mass spectrometry to in situ U–Pb zircon geochronology. *Chemical Geology*, *211*(1-2), 47–69.
Jammes, S., Manatschal, G., Lavier, L., & Masini, E. (2009). Tectonosedimentary evolution related to extreme crustal thinning ahead of a propagating ocean: Example of the western Pyrenees. *Tectonics*, *28*, TC4012. https://doi.org/10.1029/2008TC002406
Jolivet, L., Gorini, C., Smit, J., & Leroy, S. (2015). Continental breakup and the dynamics of rifting in back-arc basins: The Gulf of Lion margin. *Tectonics*, *34*, 662–679. https://doi.org/10.1002/2014TC003570
Lagabrielle, Y., & Bodinier, J. L. (2008). Submarine reworking of exhumed subcontinental mantle rocks: field evidence from the Lherz peridotites, French Pyrenees. *Terra Nova*, *20*(1), 11–21.
Lagabrielle, Y., Clerc, C., Vauchez, A., Lahfid, A., Labaume, P., Azambre, B., et al. (2016). Very high geothermal gradient during mantle exhumation recorded in mylonitic marbles and carbonate breccias from a Mesozoic Pyrenean palaeomargin (Lherz area, North Pyrenean Zone, France). *Comptes Rendus Géoscience*, *348*(3–4), 290–300. https://doi.org/10.1016/j.crte.2015.11.004
Lagabrielle, Y., Labaume, P., & de Saint Blanquat, M. (2010). Mantle exhumation, crustal denudation, and gravity tectonics during Cretaceous rifting in the Pyrenean realm (SW Europe): Insights from the geological setting of the lherzolite bodies. *Tectonics*, *29*, TC4012. https://doi.org/10.1029/2009TC002588
Lavier, L. L., & Manatschal, G. (2006). A mechanism to thin the continental lithosphere at magma-poor margins. *Nature*, *440*(7082), 324–328. https://doi.org/10.1038/nature04608
Légier, C., Tempier, C., & Vauchez, A. (1987). Tectonique tangentielle ductile syn-métamorphe d'âge crétacé supérieur dans la couverture du massif de l'Agly (zone Nord-Pyrénéenne Orientale). *Comptes Rendus. Académie des Sciences*, *305*, 907–911.
Ludwig, K. R. (2012). *Isoplot/Ex, v. 3.75, Berkeley Geochronology Center Special Publication*, (Vol. 5).
Ludwig, K. R., & Mundil, R. (2002). Extracting reliable U-Pb ages and errors from complex populations of zircons from Phanerozoic tuffs. J. Conf. Abstr. 12th Goldschmidt Conf. 2002.
Luvizotto, G. L., Zack, T., Meyer, H. P., Ludwig, T., Triebold, S., Kronz, A., et al. (2009). Rutile crystals as potential trace element and isotope mineral standards for microanalysis. *Chemical Geology*, *261*(3–4), 346–369. https://doi.org/10.1016/j.chemgeo.2008.04.012
Manatschal, G. (2004). New models for evolution of magma-poor rifted margins based on a review of data and concepts from West Iberia and the Alps. *International Journal of Earth Sciences*, *93*(3), 432–466.

Manatschal, G., Lavier, L., & Chenin, P. (2015). The role of inheritance in structuring hyperextended rift systems: Some considerations based on observations and numerical modeling. *Gondwana Research*, *27*(1), 140–164. https://doi.org/10.1016/j.gr.2014.08.006

Margalef, A., Castiñeiras, P., Casas, J. M., Navidad, M., Liesa, M., Linnemann, U., et al. (2016). Detrital zircons from the Ordovician rocks of the Pyrenees: Geochronological constraints and provenance. *Tectonophysics*, *681*, 124–134. https://doi.org/10.1016/j.tecto.2016.03.015

Marsh, J. H., & Stockli, D. F. (2015). Zircon U–Pb and trace element zoning characteristics in an anatectic granulite domain: Insights from LASS-ICP-MS depth profiling. *Lithos*, *239*, 170–185. https://doi.org/10.1016/j.lithos.2015.10.017

Masini, E., Manatschal, G., Tugend, J., Mohn, G., & Flament, J. M. (2014). The tectono-sedimentary evolution of a hyper-extended rift basin: The example of the Arzacq–Mauléon rift system (Western Pyrenees, SW France). *International Journal of Earth Sciences*, *103*(6), 1569–1596. https://doi.org/10.1007/s00531-014-1023-8

Mezger, J. E., & Gerdes, A. (2016). Early Variscan (Visean) granites in the core of central Pyrenean gneiss domes: implications from laser ablation U-Pb and Th-Pb studies. *Gondwana Research*, *29*(1), 181–198.

Mohn, G., Manatschal, G., Beltrando, M., Masini, E., & Kusznir, N. (2012). Necking of continental crust in magma-poor rifted margins: Evidence from the fossil Alpine Tethys margins. *Tectonics*, *31*, TC1012. https://doi.org/10.1029/2011TC002961

Monie, P., Soliva, J., Brunel, M., & Maluski, H. (1994). Les cisaillements mylonitiques du granite de Millas (Pyrenees, France); age Cretace 40 Ar/39 Ar et interpretation tectonique. *Bulletin de la Société Géologique de France*, *165*(6), 559–571.

Montigny, R., Azambre, B., Rossy, M., & Thuizat, R. (1986). K-Ar study of cretaceous magmatism and metamorphism in the pyrenees: Age and length of rotation of the Iberian Peninsula. *Tectonophysics*, *129*(1–4), 257–273. https://doi.org/10.1016/0040-1951(86)90255-6

Mouthereau, F., Filleaudeau, P. Y., Vacherat, A., Pik, R., Lacombe, O., Fellin, M. G., et al. (2014). Placing limits to shortening evolution in the Pyrenees: Role of margin architecture and implications for the Iberia/Europe convergence. *Tectonics*, *33*, 2283–2314. https://doi.org/10.1002/2014TC003663

Odlum, M., & Stockli, D. F. (2017). Thermotectonic evolution of the North Pyrenean Agly Massif from hyperextension through inversion using multi-mineral thermochronometry. In EGU General Assembly Conference Abstracts (Vol. 19, p. 11277).

Olivier, P. (2013). Comment on "Preorogenic exhumation of the North Pyrenean Agly massif (Eastern Pyrenees-France)" by A. Vauchez et al. *Tectonics*, *32*, 821–822. https://doi.org/10.1002/tect.20049

Olivier, P. (2015). Comment on "Thermal control on the modes of crustal thinning leading to mantle exhumation: Insights from the Cretaceous Pyrenean hot paleomargins" by Clerc and Lagabrielle. *Tectonics*, *34*, 2271–2274. https://doi.org/10.1002/2013TC003471

Olivier, P., Gleizes, G., & Paquette, J.-L. (2004). Gneiss domes and granite emplacement in an obliquely convergent regime: New interpretation of the Variscan Agly Massif (Eastern Pyrenees, France). In D. L. Whitney, C. Teyssier, & C. S. Siddoway (Eds.), *Geol. Soc. Am. Special Paper*, (Vol. 380, pp. 229–242).

Olivier, P., Gleizes, G., Paquette, J. L., & Muñoz Sáez, C. (2008). Structure and U–Pb dating of the Saint-Arnac pluton and the Ansignan charnockite (Agly Massif): A cross-section from the upper to the middle crust of the Variscan Eastern Pyrenees. *Journal of the Geological Society*, *165*(1), 141–152. https://doi.org/10.1144/0016-76492006-185

Oosthuyzen, E. J., & Burger, A. J. (1973). The suitability of apatite as an age indicator by the uranium-lead isotope method. *Earth and Planetary Science Letters*, *18*(1), 29–36. https://doi.org/10.1016/0012-821X(73)90030-7

Paquet, J., & Mansy, J. L. (1991). La structure de l'Est des Pyrénées (transversales du massif de l'Agly): un exemple d'amincissement crustal. *Comptes rendus de l'Académie des sciences. Série 2, Mécanique, Physique, Chimie, Sciences de l'univers, Sciences de la Terre*, *312*(8), 913–919.

Paquette, J. L., Gleizes, G., Leblanc, D., & Bouchez, J. L. (1997). The granite of Bassiès (Pyrenees): a syntectonic pluton of Westphalian age. U-Pb geochronology on zircons. *Proceedings of the Academy of Sciences. Series 2. Earth and Planet Sciences*, *324*(5), 387–392.

Paton, C., Hellstrom, J., Paul, B., Woodhead, J., & Hergt, J. (2011). Iolite: Freeware for the visualisation and processing of mass spectrometric data. *Journal of Analytical Atomic Spectrometry*, *26*(12), 2508–2518. https://doi.org/10.1039/c1ja10172b

Pérez-Gussinyé, M., & Reston, T. J. (2001). Rheological evolution during extension at nonvolcanic rifted margins: Onset of serpentinization and development of detachments leading to continental breakup. *Journal of Geophysical Research*, *106*(B3), 3961–3975. https://doi.org/10.1029/2000JB900325

Péron-Pinvidic, G., & Manatschal, G. (2009). The final rifting evolution at deep magma-poor passive margins from Iberia-Newfoundland: A new point of view. *International Journal of Earth Sciences*, *98*(7), 1581–1597. https://doi.org/10.1007/s00531-008-0337-9

Péron-Pinvidic, G., & Manatschal, G. (2010). From microcontinents to extensional allochthons: witnesses of how continents rift and break apart? *Petroleum Geoscience*, *16*, 189–197. https://doi.org/10.1144/1354-079309-903

Péron-Pinvidic, G., Manatschal, G., Minshull, T. A., & Sawyer, D. S. (2007). Tectonosedimentary evolution of the deep Iberia-Newfoundland margins: Evidence for a complex breakup history. *Tectonics*, *26*, TC2011. https://doi.org/10.1029/2006TC001970

Petrus, J. A., & Kamber, B. S. (2012). VizualAge: A novel approach to laser ablation ICP-MS U-Pb geochronology data reduction. *Geostandards and Geoanalytical Research*, *36*(3), 247–270. https://doi.org/10.1111/j.1751-908X.2012.00158.x

Postaire, B. (1984). *Systématique Pb commun et U-Pb sur zircons: Applications aux roches de haut grade métamorphique impliquées dans la chaîne hercynienne (Europe de l'ouest) et aux granulites de Laponie (Finlande)*, *Mémoires de la Société Géologique et Minéralogique de Bretagne*, (Vol. 15, pp. 29–72).

Poujol, M., Boulvais, P., & Kosler, J. (2010). Regional-scale Cretaceous albitization in the Pyrenees: Evidence from in situ U–Th–Pb dating of monazite, titanite and zircon. *Journal of the Geological Society*, *167*(4), 751–767. https://doi.org/10.1144/0016-76492009-144

Puigdefàbregas, C., & Souquet, P. (1986). Tecto-sedimentary cycles and depositional sequences of the Mesozoic and Tertiary from the Pyrenees. *Tectonophysics*, *129*(1-4), 173–203.

Respaut, J. P., & Lancelot, J. R. (1983). Datation de la mise en place synmétamorphe de la charnockite d'Ansignan (massif de l'Agly) par la méthode U/Pb sur zircons et monazites. In *Neues Jahrbuch für Mineralogie, Abhandlungen*. Abhandlungen: Neues Jahrbuch für Mineralogie (Vol. 147, pp. 21–34).

Reston, T. J. (1988). Evidence for shear zones in the lower crust offshore Britain. *Tectonics*, *7*(5), 929–945.

Reston, T. J. (2009). The extension discrepancy and syn-rift subsidence deficit at rifted margins. *Petroleum Geoscience*, *15*(3), 217–237. https://doi.org/10.1144/1354-079309-845

Reston, T. J., & McDermott, K. G. (2011). Successive detachment faults and mantle unroofing at magma-poor rifted margins. *Geology*, *39*(11), 1071–1074. https://doi.org/10.1130/G32428.1

Roubault, M., Leutwein, F., & Sonet, J. (1963). Geologie-mise en evidence de quatre ages apparents dans les massifs granitiques et les series cristallophylliennes des Pyrenees. *Comptes Rendus Hebdomadaires des Séances de l'Académie des Sciences*, *257*(25), 3786.

Schoene, B. (2014). 4.10-U–Th–Pb geochronology. *Treatise on geochemistry*, *4*, 341–378.

Schoene, B., & Bowring, S. A. (2006). U–Pb systematics of the McClure Mountain syenite: thermochronological constraints on the age of the 40 Ar/39 Ar standard MMhb. *Contributions to Mineralogy and Petrology*, *151*(5), 615.
Schoene, B., & Bowring, S. A. (2007). Determining accurate temperature–time paths from U–Pb thermochronology: An example from the Kaapvaal craton, southern Africa. *Geochimica et Cosmochimica Acta*, *71*(1), 165–185. https://doi.org/10.1016/j.gca.2006.08.029
Seymour, N. M., Stockli, D. F., Beltrando, M., & Smye, A. J. (2016). Tracing the thermal evolution of the Corsican lower crust during Tethyan rifting. *Tectonics*, *35*, 2439–2466. https://doi.org/10.1002/2016TC004178
Sláma, J., Košler, J., Condon, D. J., Crowley, J. L., Gerdes, A., Hanchar, J. M., et al. (2008). Plešovice zircon—A new natural reference material for U–Pb and Hf isotopic microanalysis. *Chemical Geology*, *249*(1–2), 1–35. https://doi.org/10.1016/j.chemgeo.2007.11.005
Smye, A. J., & Stockli, D. F. (2014). Rutile U–Pb age depth profiling: A continuous record of lithospheric thermal evolution. *Earth and Planetary Science Letters*, *408*, 171–182.
Sutra, E., & Manatschal, G. (2012). How does the continental crust thin in a hyperextended rifted margin? Insights from the Iberia margin. *Geology*, *40*(2), 139–142. https://doi.org/10.1130/G32786.1
Teixell, A., Labaume, P., & Lagabrielle, Y. (2016). The crustal evolution of the west-Central Pyrenees revisited: Inferences from a new kinematic scenario. *Comptes Rendus Geoscience*, *348*(3–4), 257–267. https://doi.org/10.1016/j.crte.2015.10.010
Tera, F., & Wasserburg, G. J. (1972). U-Th-Pb systematics in three Apollo 14 basalts and the problem of initial Pb in lunar rocks. *Earth and Planetary Science Letters*, *14*(3), 281–304. https://doi.org/10.1016/0012-821X(72)90128-8
Ternois, S., Odlum, M., Ford, P. R., Stockli, D. M., Tibari, B., Vacherat, A., & Bernard, B. (2019). Thermochronological evidence of early orogenesis, eastern Pyrenees, France. *Tectonics*. *106*. https://doi.org/10.1029/2018TC005254
Thomson, S. N., Gehrels, G. E., Ruiz, J., & Buchwaldt, R. (2012). Routine low-damage apatite U-Pb dating using laser ablation–multicollector–ICPMS. *Geochemistry, Geophysics, Geosystems*, *13*, Q0AA21. https://doi.org/10.1029/2011GC003928
Tomkins, H. S., Powell, R., & Ellis, D. J. (2007). The pressure dependence of the zirconium-in-rutile thermometer. *Journal of metamorphic Geology*, *25*(6), 703–713. https://doi.org/10.1111/j.1525-1314.2007.00724.x
Triebold, S., von Eynatten, H., & Zack, T. (2012). A recipe for the use of rutile in sedimentary provenance analysis. *Sedimentary Geology*, *282*, 268–275.
Tugend, J., Manatschal, G., & Kusznir, N. J. (2015). Spatial and temporal evolution of hyperextended rift systems: Implication for the nature, kinematics, and timing of the Iberian-European plate boundary. *Geology*, *43*(1), 15–18. https://doi.org/10.1130/G36072.1
Tugend, J., Manatschal, G., Kusznir, N. J., Masini, E., Mohn, G., & Thinon, I. (2014). Formation and deformation of hyperextended rift systems: Insights from rift domain mapping in the Bay of Biscay-Pyrenees. *Tectonics*, *33*, 1239–1276. https://doi.org/10.1002/2014TC003529
Vacherat, A., Mouthereau, F., Pik, R., Bellahsen, N., Gautheron, C., Bernet, M., et al. (2016). Rift-to-collision transition recorded by tectonothermal evolution of the northern Pyrenees. *Tectonics*, *35*, 907–933. https://doi.org/10.1002/2015TC004016
Vacherat, A., Mouthereau, F., Pik, R., Bernet, M., Gautheron, C., Masini, E., et al. (2014). Thermal imprint of rift-related processes in orogens as recorded in the Pyrenees. *Earth and Planetary Science Letters*, *408*, 296–306. https://doi.org/10.1016/j.epsl.2014.10.014
Vauchez, A., Chauvet, A., Lagabrielle, Y., Mainprice, D., Bestani, L., Clerc, C., & Lahfid, A. (2013). Reply to comment by P. Olivier on "Preorogenic exhumation of the North Pyrenean Agly Massif (Eastern Pyrenees, France)". *Tectonics*, *32*, 823–826. https://doi.org/10.1002/tect.20061
Vauchez, A., Clerc, C., Bestani, L., Lagabrielle, Y., Chauvet, A., Lahfid, A., & Mainprice, D. (2013). Preorogenic exhumation of the North Pyrenean Agly massif (Eastern Pyrenees-France). *Tectonics*, *32*, 95–106. https://doi.org/10.1002/tect.20015
Velasque, P. C., Ducasse, L., Muller, J., & Scholten, R. (1989). The influence of inherited extensional structures on the tectonic evolution of an intracratonic chain: The example of the Western Pyrenees. *Tectonophysics*, *162*(3–4), 243–264. https://doi.org/10.1016/0040-1951(89)90247-3
Vergés, J., & García Senz, J. M. (2001). Mesozoic Evolution and Cenozoic Inversion of the Pyrenean Rift. In P. A. Ziegler, W. Cavazza, A. H. F. Robertson, & S. Crasquin-Soleau (Eds.), *Peri-Tethys Memoir 6: Pery-Tethyan Rift/Wrench Basins and Passive Margins* (Vol. 186, pp. 187–212). Paris: Mémoires Muséum Nationald'Histore Naturelle.
Vermeesch, P. (2012). On the visualisation of detrital age distributions. *Chemical Geology*, *312*, 190–194.
Vielzeuf D (1984) Relations de phases dans le facies granulite et implications geodynamiques. L'exemple des granulites des Pyrenees. Annales Scientifiques Universit6 Clermont II Vol 79:189
Vielzeuf, D. (1996). Les massifs nord-pyrénéens à soubassement granulitique. In D., Barnolas & J. C., Chiron (Eds.), *Synthèse géologique et géophysique des Pyrénées. Introduction. Géophysique* (Vol. 1, pp. 502–521). Orléans, France: Cycle hercynien, BRGM–ITGE.
Vissers, R. L. M. (1992). Variscan extension in the Pyrenees. *Tectonics*, *11*(6), 1369–1384. https://doi.org/10.1029/92TC00823
Vry, J. K., & Baker, J. A. (2006). LA-MC-ICPMS Pb–Pb dating of rutile from slowly cooled granulites: Confirmation of the high closure temperature for Pb diffusion in rutile. *Geochimica et Cosmochimica Acta*, *70*(7), 1807–1820. https://doi.org/10.1016/j.gca.2005.12.006
Whitmarsh, R. B., Manatschal, G., & Minshull, T. A. (2001). Evolution of magma-poor continental margins from rifting to seafloor spreading. *Nature*, *413*(6852), 150–154. https://doi.org/10.1038/35093085
Wickham, S. M., & Oxburgh, E. R. (1986). A rifted tectonic setting for Hercynian high-thermal gradient metamorphism in the Pyrenees. *Tectonophysics*, *129*(1–4), 53–69. https://doi.org/10.1016/0040-1951(86)90245-3
Wiedenbeck, M., Alle, P., Corfu, F., Griffin, W. L., Meier, M., Oberli, F., et al. (1995). Three natural zircon standards for U-Th-Pb, Lu-Hf, trace element and REE analyses. *Geostandards Newsletter*, *19*(1), 1–23. https://doi.org/10.1111/j.1751-908X.1995.tb00147.x
Williams, I. S., Fiannacca, P., Cirrincione, R., & Pezzino, A. (2012). Peri-Gondwanan origin and early geodynamic history of NE Sicily: A zircon tale from the basement of the Peloritani Mountains. *Gondwana Research*, *22*(3–4), 855–865. https://doi.org/10.1016/j.gr.2011.12.007
Zack, T., Stockli, D. F., Luvizotto, G. L., Barth, M. G., Belousova, E., Wolfe, M. R., & Hinton, R. W. (2011). In situ U–Pb rutile dating by LA-ICP-MS: 208 Pb correction and prospects for geological applications. *Contributions to Mineralogy and Petrology*, *162*(3), 515–530. https://doi.org/10.1007/s00410-011-0609-4

Erratum

In the originally published version of this article, Figures 3–6 did not appear in the correct order. The figure numbers and placement as well as several figure citations have now been corrected, and this version may be considered the authoritative version of record.